Development, Generation and Origin of Synchronous Oscillations in the Brainstem Respiratory Network

Joy Yoshiko Sebe

A dissertation
submitted in partial fulfillment of the
requirements for the degree of

Doctor of Philosophy

University of Washington

2006

Program Authorized to Offer Degree:
Neurobiology and Behavior

University of Washington
Graduate School

This is to certify that I have examined this copy of a doctoral dissertation by

Joy Yoshiko Sebe

and have found that it is complete and satisfactory in all respects,
and that any and all revisions required by the final
examining committee have been made.

Chair of the Supervisory Committee:

Albert J. Berger

Reading Committee:

Albert J. Berger

Jane M. Sullivan

David J. Perkel

Date: November 29, 2006

In presenting this dissertation in partial fulfillment of the requirements for the doctoral degree at the University of Washington, I agree that the Library shall make its copies free available for inspection. I further agree that extensive copying of the dissertation is allowable only for scholarly purposes, consistent with "fair use" as prescribed in the U.S. Copyright Law. Requests for copying or reproduction of this dissertation may be referred to ProQuest Information and Learning, 300 North Zeeb Road, Ann Arbor, MI 48106-1346, 1-800-521-0600, to whom the author has granted "the right to reproduce and sell (a) copies of the manuscript in microform and/or (b) printed copies of the manuscript made from microform."

Signature 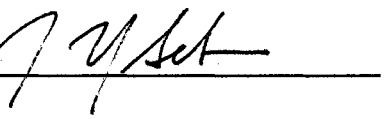

Date 12/6/06

University of Washington

Abstract

Development, generation and origin of synchronous oscillations in the brainstem respiratory network

Joy Yoshiko Sebe

Chair of the Supervisory Committee:
Professor Albert J. Berger
Department of Physiology and Biophysics

Neurons within the intact respiratory network are synchronized on long and short time scales to generate respiratory rhythm and synchronous oscillations in spike firing during inspiration (Figure 1.1), respectively. Such oscillations shape the pattern of inspiratory activity that leads to contractions of the inspiratory muscles. By recording inspiratory activity from the rhythmically mouse medullary slice, I investigated synchronous oscillations during postnatal development (P0-11), the role of inhibitory synaptic transmission in generating oscillations and examined where in the slice oscillations are produced.

I found that average oscillation frequency significantly increased with postnatal development. Bath application of $GABA_A$ and GlyR antagonists significantly reduced synchronous oscillation power and increased peak integrated activity of inspiratory bursts in both neonates and juveniles. Bath application of Substance P alone, while increasing peak integrated activity, had no significant effect on oscillation power. Prolonging the time course of GABAergic synaptic currents with zolpidem decreased the median oscillation frequency. These data demonstrate that oscillation frequency increases with postnatal development and that both GABAergic and glycinergic

transmission contribute to synchronization of motoneuron activity. Further, the time course of synaptic GABAergic currents is a determinant of oscillation frequency.

Next, I tested the PreBötzinger Complex (PBC) and the XII nucleus as candidate regions in which oscillations are produced. Unilateral excitation of the PBC, via local perfusion of ACSF containing high K^+, increased inspiratory burst frequency bilaterally, but had no effect on oscillation power recorded bilaterally. In contrast, unilateral excitation of the XII nucleus increased peak integrated activity bilaterally and oscillation power in the ipsilateral XII rootlet. Crosscorrelation analysis of control inspiratory activity recorded from the left and right XII rootlets produced crosscorrelation histograms with broad, significant peaks centered around a time lag of zero and no harmonic peaks. Coherence analysis of control left and right XII rootlet recordings demonstrated that oscillations are only weakly coherent. Together these data indicate that inspiratory-phase synchronous oscillations are generated in or immediately upstream of the XII motor nucleus. Collectively, my thesis research demonstrates a mechanism underlying the generation of synchronous oscillations and proposes a region of the simplified respiratory network in which these oscillations are produced.

TABLE OF CONTENTS

LIST OF FIGURES

Acknowledgements

The support of numerous people has enabled me to start and complete my dissertation.

I would like to thank my advisor, Albert Berger, for his conscientious mentoring, his enthusiasm for my thesis research, and his sincere interest in my personal well-being. I would also like to thank the members of my Supervisory Committee, Jane Sullivan, Randy Powers, Marti Bosma and David Perkel, who cultivated my scientific and professional development through numerous one-on-one discussions and during the many stages of my graduate career.

In the lab, Hans vanBrederode's suggestions have often made the difference between my experimental success and failure and have saved me many months of work. Bill Satterthwaite has provided constant technical assistance. The experiences that Albert, Hans and Bill have shared with me with respect to their roles as husbands and fathers have given me much to look forward to in the near future. I would also like to thank past members of the Berger Lab including Erika Eggers, Rebecca Lim, Priscilla Hoang, Parker Haley, Jennifer O'Brien and Phan Huynh for their friendship, comic relief and helpful discussions.

Throughout the years, Seattle has felt more and more like home because of the friendships that I developed while living here. Although, I cannot name all of the people whose friendships have enriched my life during graduate school, I would like to acknowledge a number of people in particular for their warmth, humor and thoughtfulness. They are Stephanie Krasnow, April Bragg, Shallin Busch, Michelle Fisher, Tara Fletcher, Debika Shome, Abby Person, Sarah Albano and Hiro Watari.

Graduate school is an important landmark on a continuum of my life's endeavors. My mother and father, Akira and Sumiko Sebe, and my sister, Delphine Sebe, have provided unyielding love and support until now and they will continue to do the same, particularly as I try to balance my professional and family lives. The Detwiler Family, particularly Daryl and Elaine Detwiler, have wholeheartedly welcomed me into their family and are credited with raising my most enthusiastic and constant cheerleader, my husband Jason Detwiler. Jason has always been and will always be my tireless supporter throughout our life together. I can only strive to provide the same for him. Lastly, I would like to thank my son-in-the-making simply for growing.

Dedication

To my family

Chapter 1: General Introduction

Synchronous oscillations of brain activity have been described almost ubiquitously in the mammalian brain and span a wide range of time scales. Synchrony on a millisecond time scale, which generates 2-100 Hz oscillations, has been implicated in a myriad of functions, such as memory (Seager et al., 2002; Kahana 2006) and sensory processing (Stopfer et al., 1997; Gelperin 2006), sleep (Steriade et al., 1993) and movement (Baker and Baker 2003). On a longer time scale, neurons within the brainstem and spinal cord generate slower rhythms that are critical for vital bodily functions such as respiration. Inspiratory motoneurons within the brainstem respiratory network exhibit both fast and slow oscillations that are a product of short and long time scale synchrony, respectively. Inspiratory rhythm is characterized by regularly occurring bursts of action potentials, or inspiratory bursts, that are each followed by a period of quiescence. Not only are these bursts a product of long time scale synchrony, but they are bilaterally synchronized to yield contractions in the left and right sides of the inspiratory muscles. Inspiratory neurons are further synchronized on a short time scale to generate fast oscillations that occur within an inspiratory burst.

I have examined short time scale, long time scale and bilateral synchrony exhibited by inspiratory motoneurons of the *in vitro* rodent brainstem respiratory network. I elucidated a synaptic mechanism underlying the generation and time course of short time scale synchrony and have examined this during postnatal development. In the latter part of my thesis work, I determined which neuronal populations within the *in vitro* respiratory network play an important role in enhancing short time scale synchrony and investigated the bilateral synchrony of inspiratory-phase discharge.

Synchrony, Oscillations and Synchronous Oscillations

Synchrony, oscillations and synchronous oscillations are three distinct forms of neural activity although these terms are sometimes used synonymously. Synchrony does not imply oscillatory activity and oscillations are not necessarily synchronous across multiple neurons. *Synchrony* occurs when 2 or more neurons that are electrically and/or chemically coupled exhibit the same changes in membrane potential such as subthreshold depolarizations and hyperpolarizations and spike firing. *Oscillations* are either subthreshold or suprathreshold changes in membrane potentials, exhibited by a single neuron, within a particular frequency range. *Synchronous oscillations* are produced when 2 or more neurons that are electrically and chemically coupled exhibit temporally correlated subthreshold or suprathreshold changes in their membrane potentials. Due to the widespread nature of synchronous oscillations in the mammalian brain, the term *oscillations* is commonly used to refer to synchronous oscillations.

Long Time Scale, Short Time Scale and Bilateral Synchrony

In my thesis work, I have investigated three different forms of neural synchrony in the inspiratory network that are termed long time scale, short time scale and bilateral synchrony. Long time scale synchrony refers to the synchronized spike firing and periods of quiescence exhibited by inspiratory neurons on a time scale of hundreds of milliseconds to several seconds. Inspiratory rhythm is produced by inspiratory neurons that are synchronized on a long time scale to fire bursts of action potentials that are separated by regular intervals of no activity (Figure 2.6A and B). Short time scale synchrony refers to the spike firing and periods of little or no activity that occurs on a

millisecond time scale. During an inspiratory burst, inspiratory motoneuron firing is synchronized on a short time scale to produce regularly recurring clusters of action potentials that are separated by periods of little or no activity (Figure 1.1). This pattern of inspiratory phase firing is referred to as inspiratory-phase synchronous oscillations. Bilateral synchrony occurs on both long and short time scales in the inspiratory network. That is, inspiratory rhythm (Figure 3.1B and 3.2B) and synchronous oscillations (Cohen et al., 1997) recorded from the left and right sides of the inspiratory network, often from the inspiratory nerves, are temporally correlated. The inspiratory network serves as an excellent model with which to study neural synchrony, and the one which I have chosen for my thesis research, because long time scale, short time scale and bilateral synchrony have exclusively been observed during the inspiratory phase of the respiratory rhythm (Mitchell and Herbert 1974; Smith et al., 1991; Li et al., 2003).

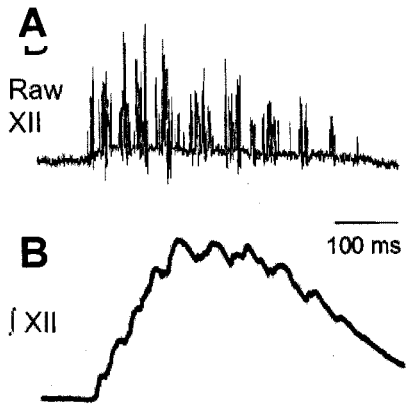

Figure 1.1 Inspiratory-phase synchronous oscillations. A. The raw hypoglossal nerve recording (Raw XII) shows the clusters of action potentials that are separated by gaps of little or no activity. B. The corresponding rectified and integrated trace (∫XII) reveals the oscillatory nature of this synchronous activity within an inspiratory burst. Note the periodic waves that ride on the overall envelope of the rectified and integrated hypoglossal nerve trace are a consequence of these synchronous oscillations.

Inspiratory Rhythm Generation

We depend on our respiratory system to live, yet the majority of us seldomly think about the neural activity responsible for respiration. Mammalian respiration is driven by a composite of multiple neural rhythms (ie. inspiratory, post-inspiratory, expiratory) (Richter 1982) but the most commonly discussed are the inspiratory and expiratory rhythms. Inspiratory rhythm is generated in the brainstem, propagated to inspiratory motoneurons in the brainstem and spinal cord, and leads to contractions of inspiratory muscles such as the diaphragm and tongue. Expiration also arises from the brainstem, but is out of phase with respect to inspiration and leads to contractions in expiratory muscles such as the internal intercostal muscles of the ribcage (Hlastala and Berger 2001). For centuries, the region of the brainstem that generates inspiratory rhythm eluded scientific discovery. In 1991, Smith and colleagues (Smith et al., 1991) reported that they had found the locus of mammalian respiratory rhythm generation in the ventral medulla. They named this region the PreBötzinger Complex (PBC) and hypothesized that respiratory rhythm is driven by pacemaker neurons in the PBC. In subsequent studies, Smith's laboratory further supported this conclusion by demonstrating that inspiratory rhythm is driven by pacemaker neurons, within the PBC, that express a riluzole sensitive persistent Na^+ current (I_{NaP}) (Del Negro et al., 2002). We now know that inspiratory rhythm is generated by two types of PBC pacemakers neurons, those expressing I_{NaP} and another population of neurons that expresses a cadmium sensitive inward current (Thoby-Brisson and Ramirez 2001; Del Negro et al., 2005). Although many studies of the PBC aim to characterize pacemaker neuron properties, the PBC is also composed of inspiratory non-pacemaker neurons. In fact, electrophysiological sampling of individual PBC neurons have shown that less than

10% of sampled PBC neurons are pacemaker neurons (Del Negro et al., 2002; Pena et al., 2004).

Until recently, it was widely accepted that inspiratory rhythm generated in the PBC drives the multiple rhythms that compose respiratory rhythm. According to this theory, expiratory neurons are inhibited during inspiration and fire during the quiescent phase of inspiratory rhythm when expiratory neurons are released from synaptic inhibition. Recently, two independent research groups have presented new conflicting theories with regard to the source of respiratory rhythm generation. Since 2003, Feldman has posited that two different but coupled oscillators in the PBC and the parafacial respiratory group (pFRG) generate the inspiratory and expiratory rhythms, respectively (Mellen et al., 2003; Janczewski and Feldman 2006). Homma, on the other hand, purports that the pre-inspiratory neurons of the pFRG, located rostral to the PBC, generates the respiratory rhythm to which the inspiratory rhythm is entrained (Onimaru et al., 2006). Although both groups refer to overlapping publications (Mellen et al., 2003; Onimaru et al., 2006), it is interesting how different their conclusions are.

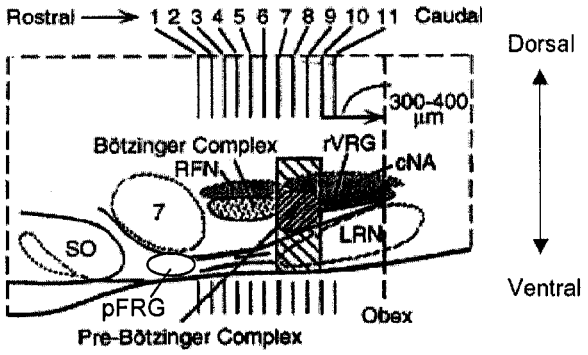

Figure 1.2. Sagittal view of the medulla showing the location of the Botzinger Complex, PreBötzinger Complex (PBC) and the neighboring regions (SO, superior olive; 7, facial nucleus; pFRG, parafacial respiratory group; LRN, lateral reticular nucleus; RFN, retrofacial nucleus; rVRG, rostral ventral respiratory group; cNA, caudal (semicompact division) of nucleus ambiguus). The rhythmically active medullary slice preparation must include the hatched rectangular area which indicates the region necessary for inspiratory rhythmogenesis. Taken from Smith et al. (1991)

Neither group has presented conclusive evidence that disproves the theory, established over fifteen year period of sound publications, that the PBC is the inspiratory rhythm generator.

In Vitro Approaches to Studying Inspiratory Activity

The foundational research in respiratory neurobiology was performed using *in vivo* preparations such as the anesthetized cat, dog and rabbit (von Euler 1986). One of the goals of these *in vivo* studies was to determine the location of the central pattern generator for respiratory rhythm. By employing lesions, brainstem transections, antidromic stimulation of respiratory nerves and microelectrode recordings, pioneers in the field were able to conclude that a central pattern generator (CPG) for respiratory rhythm was bilaterally located in the medulla. However, using *in vivo* preparations, it was difficult to identify the CPG in finer detail. By developing the rhythmically active medullary slice preparation, which I will later describe in detail, Smith et al. were able to identify the PBC as the locus of inspiratory rhythm generation (Smith et al., 1991). By sectioning the brainstem caudally, from the pontomedullary junction, and rostrally, from the spinomedullary junction, Smith et al. found that the brainstem slice generated inspiratory rhythm only if it contained a population of neurons located caudal to the so-called Bötzinger Complex (Figure 1.2). They named this region containing inspiratory rhythm generating neurons the PreBötzinger Complex. They went on to record from individual PBC neurons and identified neurons that exhibited voltage-dependent pacemaker properties. Electrophysiological studies have also demonstrated that the PBC contains pacemaker neurons that continue to generate inspiratory rhythm in the absence of synaptic inputs (Thoby-Brisson and Ramirez 2001; Tryba et al., 2003).

Subsequent studies in which the PBC was pharmacologically manipulated *in vivo* (Koshiya and Guyenet 1996; Pierrefiche et al., 1998) have confirmed this region as the inspiratory rhythm generator in the intact animal.

The development of two rodent *in vitro* preparations containing simplified respiratory networks substantially facilitated the study of inspiratory-phase activity. The first of these respiratory-related *in vitro* preparations, the brainstem-spinal cord preparation, was introduced by Suzue in 1984 (Suzue 1984). Then in 1991, Smith et al. presented the rhythmically active medullary slice preparation (Smith et al., 1991). In comparison to the *in vivo* experimental models, these *in vitro* preparations have enabled many more methodological approaches and have thus served as powerful tools with which to study the mammalian respiratory network. Aside from the obvious reason that a mouse preparation is amenable to genetic studies, the *in vitro* preparations have made neurons that are part of the respiratory network more accessible to intracellular recording, pharmacological manipulation and optical imaging.

In vivo versus *in vitro* studies also differ in the age of animals that are used. Most of the *in vivo* work, with the exception of a few developmental studies (Paton and Richter 1995a; Paton and Richter 1995b), have utilized adult animals (von Euler 1986; Ramirez et al., 2002). In contrast, the *in vitro* preparations have facilitated study of the developing respiratory network (Ramirez et al., 2002), because only small, and thereby young, animals can be used for these preparations. By using young rodents it is possible to include the essential components of the respiratory network in a thinner section of tissue that can be adequately oxygenated and from which metabolically produced carbon dioxide can be readily removed. Typically only perinatal rodents and rodents in the first two weeks of postnatal development are used for *in vitro*

preparations. In addition to the differences between *in vivo* and *in vitro* approaches to studying respiratory activity, there are also distinctions between the two different *in vitro* preparations.

The brainstem-spinal cord preparation and rhythmically active medullary slice preparation each possess unique advantages that tailor one or the other to different kinds of experiments. As the name implies, the basic brainstem-spinal cord preparation, contains parts of the brainstem and spinal cord, more specifically from the rostral pons to the sacral regions of the cord (Smith and Feldman 1987). Unlike the rhythmically active medullary slice preparation, the brainstem-spinal cord preparation contains multiple sets of inspiratory nerves of which the most commonly used to record inspiratory activity are the hypoglossal (XII) and phrenic (C4) nerves, that innervate the tongue and diaphragm, respectively. Therefore, the brainstem-spinal cord preparation can be used when one wants to record inspiratory-phase activity from phrenic motoneurons or nerves *in vitro* (Bou-Flores and Berger 2001; Parkis et al., 2003). The brainstem-spinal cord preparation is also rhythmically active at a physiological K^+ concentration (3 mM), unlike the medullary slice preparation, which requires bath application of elevated K^+ (8 mM) ACSF to sustain prolonged rhythmic activity (Smith et al., 1991; Ruangkittisakul et al., 2006). In contrast to the brainstem-spinal cord preparation, the medullary slice preparation is a thin section of the medulla (500-700 μm) (Smith et al., 1991; Sebe et al., 2006). The slice preparation is composed of a simpler circuit than the brainstem-spinal cord preparation and can be used to record inspiratory-phase activity from the PBC neurons, XII motoneurons (HMs) or XII nerves. I used the rhythmically active medullary slice to examine inspiratory-phase activity exhibited by the XII rootlets because of the advantages afforded by the reduced nature

of the preparation. Because the slice preparation is thinner and therefore less sensitive to hypoxia, it can be used to study the simplified respiratory network over a broader developmental age range than that permitted by the brainstem-spinal cord preparation. The thinner rhythmically active slice preparation also allows oxygen, pharmacological agents, and other compounds in the bath solution to readily penetrate the preparation. Regions such as the PBC and XII nucleus are located at the surface of the slice and therefore accessible to localized application of pharmacological agents. Lastly, due to the simpler circuitry in the slice preparation it is easier to determine the connections underlying synchrony in the XII motor output.

The medullary slice preparation contains the PBC, a potential intermediate premotor area, the XII nucleus, and the XII rootlets. Together, these regions form a simplified network that propagates inspiratory rhythm from the PBC to the XII nerves that innervate the tongue. A combination of immunohistochemical, imaging and electrophysiological studies have elucidated the location of and connectivity between the bilaterally located PBCs. NK1 receptor (NK1R) labeling of the slice (Gray et al., 1999) and electrophysiological recordings (Johnson et al., 2001; Li et al., 2003) have shown that the PBC is bilaterally located in the ventral lateral region of the slice. Calcium imaging has shown that PBCs on either side of the midline are synchronized by bilateral glutamatergic projections crossing near the ventral border of the slice (Koshiya and Smith 1999). Therefore, it is likely that inspiratory rhythm is bilaterally synchronized at the level of the PBC.

From the PBC, inspiratory activity propagates dorsally to the XII nucleus. The left and right sides of the XII nucleus flank the central canal and the ventral tip of the 4th ventricle. Anatomical examination of HMs have shown that the axons project ventrally

to form the XII nerve, but lack recurrent axon collateral projections (Viana et al., 1990). However, some of the HM dendrites, which project radially from the soma, cross the midline of the slice and project into the contralateral XII nucleus (Nunez-Abades et al., 1994). Tracer studies have shown that HMs in the left and right XII nuclei are coupled, likely via dendrodendritic or dendrosomatic junctions (Mazza et al., 1992). It is therefore possible that electrical coupling of HMs, mediated by midline crossing dendrites, underlies some form of bilateral synchrony.

Using the rhythmically active slice preparation, I have recorded inspiratory-phase activity from the XII rootlets to study the connections underlying bilateral synchronization. I have also examined the synchrony that results in long time scale patterns such as inspiratory rhythm, which I have already described, and short time scale patterns such as the oscillations within an inspiratory burst.

Short Time Scale Synchrony in the Inspiratory Network

On a short time-scale, respiratory motoneurons synchronously fire at a particular frequency during inspiration (Cohen et al., 1997; Funk and Parkis 2002) creating a pattern of activity that I refer to as synchronous oscillations. Dittler and Garten first reported respiratory-related synchronous oscillations in 1912 using string galvanometer recordings of cat phrenic nerve activity. Many years after these initial recordings, Cohen (Cohen 1973; Cohen et al., 1997) and others (Sears and Stagg 1976) pioneered an extensive investigation of inspiratory-phase short time scale synchrony using a range of analysis techniques (i.e. power spectral, coherence, crosscorrelation analysis).

Inspiratory-phase synchronous oscillations have now been recorded *in vivo* (Cohen et al., 1997) and *in vitro* (Funk and Parkis 2002) and from several inspiratory

motor nerves including those that innervate the diaphragm (Cohen et al., 1974; Richardson and Mitchell 1982; O'Neal, III et al., 2005), tongue (Cohen et al., 1987; Bou-Flores and Berger 2001), and laryngeal muscles (Richardson and Mitchell 1982). The properties of synchronous oscillations, such as their frequency, amplitude and coherence across different neuronal populations, have been well characterized.

In the 15-120 Hz range within which synchronous oscillations occur, there are two categories of oscillations, medium and high frequency oscillations (MFOs and HFOs, respectively). Oscillations can be differentiated into one of these two categories according to their frequency range and, more reliably, by the region of the brainstem or spinal cord in which they are generated (Cohen et al., 1997; Funk and Parkis 2002). According to the former criterion, MFOs are observed within the 15-50 Hz frequency range whereas HFOs are usually recorded within the 50-120 Hz range. However, oscillation frequency is dependent upon changes in temperature (Dittler and Garten 1912; Richardson and Mitchell 1982), hypercapnia, anesthetics, on the preparation used (Funk and Parkis 2002) and the age of the animal studied (Suthers et al., 1977). With respect to the latter criterion, HFOs recorded bilaterally in the same inspiratory motoneuron population (ie. left and right phrenic nerves) and across different inspiratory nerves (ie. phrenic vs. recurrent laryngeal) show strong coherence, suggesting that they are generated by common inputs from medullary neurons (Richardson and Mitchell 1982). In contrast, MFOs show little or no coherence when recorded from bilateral nerves from the same motoneuron population and no coherence when recorded from different inspiratory nerves, which indicates that they are generated at or immediately upstream of the motoneuron level (Cohen et al., 1987). Therefore, it is probable that

HFOs and MFOs are generated in different, yet to be identified, regions of the respiratory network.

Despite our extensive knowledge regarding inspiratory-phase synchronous oscillation properties, we know less about the synaptic connections and neural mechanisms by which they are generated. Insight into the potential neural mechanisms underlying synchronous oscillations in the respiratory network can be gained from studies of oscillations in other brain regions.

Mechanisms Underlying Synchronous Oscillations

The mechanisms by which synchronous oscillations are generated have been examined in many brain regions, including the hippocampus (Mann et al., 2005), thalamus (Steriade 1999), and olfactory system (Gelperin 2006; Schoppa 2006). These studies have demonstrated that GABAergic and glutamatergic transmission, as well as electrical coupling, are involved in the generation of synchronous oscillations. Of these three mechanisms, $GABA_A$ receptor ($GABA_AR$) -mediated synaptic transmission plays the most critical role.

Hippocampal and olfactory bulb studies have provided direct evidence that GABAergic transmission is sufficient to initiate oscillations and is able to synchronize rhythmic spike firing. In the hippocampus, where network oscillations coincide with exploratory behavior, unitary IPSPs, produced by GABAergic interneuron stimulation, initiate subthreshold oscillations in CA1 pyramidal cells (Cobb et al., 1995). Rhythmic unitary GABAergic IPSPs are able to evoke and synchronize spike firing in simultaneously recorded pyramidal cells via post-inhibitory rebound firing. Recovery from GABAergic IPSPs also results in oscillations and spike synchrony in

simultaneously recorded mitral cells of the olfactory bulb (Schoppa 2006). In both cases, membrane hyperpolarization mediated by GABAergic IPSPs and recovery from IPSPs underlie oscillations in membrane potential. Further, GABAergic IPSPs were able to synchronize spike firing in simultaneously recorded principal neurons. Previous work from our laboratory has also shown that GABAergic and glycinergic synaptic inhibition are important in generating inspiratory-phase synchronous oscillations recorded from XII nerves of the neonatal respiratory network (Bou-Flores and Berger 2001).

In the hippocampus, GABAergic and glutamatergic synaptic transmission are required for the generation of cholinergically induced 40 Hz oscillations (Fisahn et al., 1998). Such oscillations persist in the presence of metabotropic glutamate and NMDA receptor (mGlu and NMDAR) antagonists, but are blocked following application of either $GABA_AR$ or AMPA receptor (AMPAR) antagonists. The synaptic connections between GABAergic and glutamatergic neurons that produce synchronous oscillations are still unknown. However, data from *in vitro* experiments (Fisahn et al., 1998) and hippocampal network models (Mann et al., 2005) suggest that synchronous oscillations are generated by synaptic recurrent feedback loops between excitatory principal neurons and inhibitory interneurons. An example of recurrent feedback loops that may generate synchronous oscillations in the inspiratory network is shown in Figure 1.3. According to this model, inspiratory neurons are activated during inspiration, possibly by inputs originating from pacemaker neurons, and send excitatory synaptic inputs to multiple inhibitory interneurons. These interneurons, in turn, inhibit the excitatory neurons. The alternating excitation and inhibition produced by this recurrent feedback

loop produces the clusters of action potentials and periods of no activity, respectively, that compose inspiratory-phase synchronous oscillations.

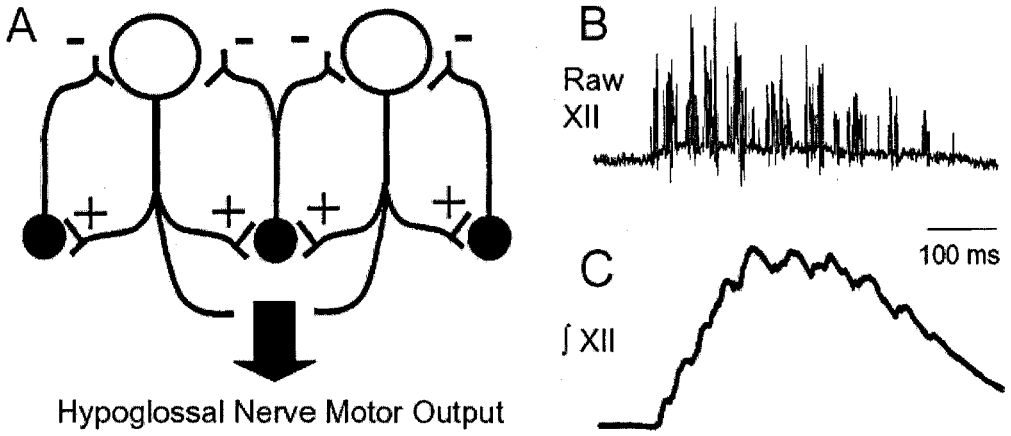

Figure 1.3 Hypothetical Model for the Generation of Synchronous Oscillations. A. During an inspiratory burst, inspiratory neurons are activated and send excitatory inputs to multiple inhibitory interneurons that, in turn, transiently inhibit inspiratory neurons. Multiple inspiratory neurons synchronously exhibit this cycle of alternating excitation and inhibition that occurs during inspiration and can be recorded from the hypoglossal nerve motor output. B. The raw hypoglossal nerve recording (Raw XII) showing inspiratory-phase synchronous oscillations. C. The corresponding rectified and integrated trace (∫XII) reveals the oscillatory nature of this synchronous activity within an inspiratory burst.

Unlike chemical synaptic transmission, electrical transmission is not required for the generation of oscillations, but is important in regulating the magnitude of synchronous oscillations. To examine the role of electrical coupling in generating hippocampal oscillations, connexin-36 knockout mice were developed that lack electrical coupling between pairs of interneurons recorded in both the dentate gyrus and CA3 region. In such mice, gamma frequency (30-80 Hz) oscillations persisted, but the amplitude of these oscillations was substantially reduced (Hormuzdi et al., 2001). Within the respiratory neural network, gap junctions blockers elicit conflicting effects on synchronous oscillations recorded from inspiratory motoneurons in neonate versus adult rodents. In the neonatal respiratory network, gap junction blockade increases the

power of synchronous oscillations (Bou-Flores and Berger 2001) but decreases the power of oscillations in the adult rodent (Solomon et al., 2003). Although the effects of gap junction blockers on inspiratory motoneuron synchronization may be developmentally and preparation dependent, both studies show that electrical coupling is involved in synchronizing inspiratory motoneuron oscillatory activity.

Based on previous studies demonstrating the need for GABAergic transmission in generating oscillations (Cobb et al., 1995; Bou-Flores and Berger 2001; Schoppa 2006), I have investigated the role of GABAergic and glycinergic transmission in generating inspiratory-phase synchronous oscillations during postnatal development.

Functional Significance of Synchronous Oscillations

Given the prominence of oscillations within the brain, one cannot help but wonder what functions these oscillations serve. One study in the honeybee olfactory system has demonstrated that synchronous oscillations are required for fine odor discrimination (Stopfer et al., 1997). Honeybees are usually able to discriminate between similar odors (i.e. 1-hexanol and 1-octanol) and dissimilar odors (i.e. an alcoholic scent from a floral scent) (Stopfer et al., 1997). When oscillations in the honeybee olfactory system are desynchronized, via application of a $GABA_AR$ antagonist (MacLeod and Laurent 1996), honeybees are no longer able to discriminate between similar odors (Stopfer et al., 1997). The discrimination of dissimilar odors, however, does not change.

The search for the functional significance of synchronous oscillations in more complex nervous systems is ongoing. Numerous experiments, using animals and humans, have demonstrated that oscillations are consistently associated with particular

behaviors depending on the brain region examined. In the thalamus, synchronous oscillations of varying frequency ranges and strengths are associated with different sleep stages and arousal states. For example, EEG recordings have shown that thalamic neurons oscillate at a frequency of 7-14 Hz during the early stage of sleep. As sleep deepens, the frequency of these oscillations decreases. During rapid eye movement sleep and dreaming episodes, low frequency oscillations are abolished and cellular excitability increases, much like during wakefulness (Steriade et al., 1993).

EEG recordings of the human brain further support the correlation between oscillations and activity. In the human sensorimotor cortex, synchronous oscillations are strongest during periods of steady contraction, but not as prominent during relaxation and in the transition from relaxation to contraction (Baker and Baker 2002). In the human hippocampus and cortex, the power of oscillations in the 4-8 Hz range increases during exploration and navigation (Ekstrom et al 2005, Caplan et al. 2003).

These and other work demonstrate an intriguing connection between oscillations and complex behaviors; however, the relationship between the two remains correlative. Although determining the physiological significance of oscillations has proved challenging, it has been easier to determine the function of oscillations with respect to simple behaviors. One study in the rabbit has shown that hippocampal oscillations can facilitate associative learning in the mammalian brain (Seager et al., 2002). Using a standard classical conditioning paradigm, Seager et al. trained one group of rabbits when they exhibited hippocampal theta oscillations and another group of rabbits when they did not. They found that rabbits trained during oscillatory activity learned in half as many trials relative to rabbits trained during non-oscillatory activity. This work by Seager et al. has demonstrated that oscillations can accelerate a simple form of

learning. However, much work is necessary to determine whether and how oscillations are involved in higher brain functions such as sleep, exploration and navigation.

Physiological Relevance of Oscillations in the Respiratory Network

The function of inspiratory-phase synchronous oscillations in the brainstem has also been investigated, although to a lesser extent relative to oscillations observed in other brain regions. Inspiratory-phase synchronous oscillations are not required for respiratory rhythm generation, but they are important in generating the pattern of inspiratory discharge. At the motoneuron level, oscillations increase the input-output efficiency of inspiratory motoneurons and the precision of spike timing. Parkis et al. recorded inspiratory-phase oscillations from rhythmically active phrenic motoneurons and injected these oscillatory currents into the same phrenic MNs (Parkis et al., 2003). They found that these endogenous current oscillations increase the number of spikes fired. Oscillatory inputs also increased the precision of phrenic motoneuron spike timing by raising the membrane potential near threshold and triggering action potentials that were coincident with oscillation peaks. Excitatory neuromodulators such as Substance P increase motoneuron excitability (Rekling et al., 2000; Yasuda et al., 2001). However, endogenous oscillatory inputs injected in the presence of a noradrenergic receptor agonist are able to constrain phrenic motoneuron firing frequency to that of control (Parkis et al., 2003). From these data, it is evident that oscillations shape the pattern of inspiratory-phase activity.

Synchronous firing of inspiratory motoneurons may also serve to increase muscle force output. Baker et al. developed a computer model in which they simulated the effect of synchronous oscillatory EPSP inputs injected into motoneurons on

electromyograms (EMGs) (Baker et al., 1999). They determined that muscle force increased as the synchrony of oscillatory inputs increased. The physiological relevance of synchronous oscillations with respect to muscle output has not been tested experimentally, but future work in this research arena will be of great interest.

Specific Aims

In the following work, I have investigated several aspects of inspiratory-phase short time scale synchrony, or synchronous oscillations, exhibited by XII nerve rootlets *in vitro*. In the first part of my thesis research, I examined changes in these synchronous oscillations during postnatal development and studied a mechanism underlying the generation and time course of these oscillations. In the latter part of my thesis research, I used the relative simplicity of the neural circuit within the rhythmically active medullary slice preparation to my advantage and determined a region in the slice within which oscillations are likely to be generated.

In the first set of experiments, I focused on the synaptic mechanisms underlying synchronous oscillations. Previous work by Bou-Flores and Berger demonstrated that inhibitory synaptic transmission is required to generate inspiratory-phase synchronous oscillations within the first week of postnatal life. Due to the changes in inhibitory synaptic transmission that occur over development, I extended this work to examine the role of inhibitory synaptic transmission in generating short time scale synchrony during a longer period of postnatal development. In studying synchronous oscillations during postnatal development, my first step was to assess changes in oscillations recorded in control condition in postnatal day 0-11 (P0-11) mice. Previous investigation of inspiratory-phase oscillation frequency in kittens and puppies demonstrated that

oscillation frequency increases as the animal develops. Therefore, I hypothesized that oscillation frequency in my preparation would increase with postnatal development.

Next, I focused on the role of inhibitory synaptic transmission in generating synchronous oscillations. Consistent with previous *in vitro* work by Bou-Flores and Berger, I hypothesized that GABAergic and glycinergic transmission are required to generate synchronous oscillations during postnatal development. To test this hypothesis, I assessed the effect of bath application of $GABA_A$ and glycine receptor (GlyR) antagonists on the power of inspiratory-phase synchronous oscillations recorded from XII nerve rootlets. Studies in the hippocampus and olfactory system have shown that GABAergic IPSPs are responsible for the trough phase of an oscillation and that the peak occurs in response to rebound from membrane hyperpolarization. If GABAergic transmission generates oscillations in the inspiratory network in the same manner (Figure 1.3), I hypothesized that prolonging the time course of inhibitory transmission would decrease oscillation frequency. To test this hypothesis, I prolonged the time course of GABAergic currents via bath application of zolpidem and measured changes in oscillation frequency. Together, these questions were aimed at understanding synchronous oscillations during postnatal development and the role of inhibitory synaptic transmission in their generation.

Having investigated a mechanism by which inspiratory-phase oscillations are generated, I next sought to determine the origin of synchronous oscillations within the slice. To do this, I employed a combination of experimental tests and data analysis techniques. First, I recorded bilateral inspiratory-phase activity from XII rootlets and unilaterally increased neuronal excitability in either the PBC or XII nucleus. Increasing the excitability of neurons in the PBC or XII nucleus should increase the number of

neurons that fire action potentials in response to oscillatory synaptic input thereby increasing the power of oscillations recorded in the XII motor output. If synchronous oscillations are generated in the PBC, locally increasing the excitability of PBC neurons should increase the power of oscillations. Given this effect, oscillation power should increase bilaterally if the connections between the left and right PBCs can synchronize activity on a short time scale. If oscillations are generated within or immediately upstream of the XII nucleus, unilateral excitation of the XII nucleus should increase the power of oscillations. Further, if the left and right XII nuclei are bilaterally connected, oscillation power should increase in the XII rootlets ipsilateral and contralateral to the side of unilateral excitation.

Next, I applied crosscorrelation and coherence analysis to categorize whether or not synchronous oscillations in the slice are temporally coincident and occur at the same frequency, respectively. If oscillations recorded from the left and right XII rootlets are temporally coincident and occur at the same frequency, they are generated by a common input source that is capable of synchronizing oscillations bilaterally (Kirkwood et al., 1982; Cohen et al., 1997). Within the rhythmic slice, this common input source corresponds to the PBC. If oscillations recorded from the left and right XII rootlets are not temporally coincident and do not occur at the same frequency, they are generated individually in the left and right hypoglossal nuclei or in the left and right premotor regions, which lie immediately upstream of the hypoglossal nuclei (Kirkwood et al., 1982; Cohen et al., 1997).

Chapter 2: Inhibitory Synaptic Transmission Governs Inspiratory Motoneuron Synchronization

Introduction

GABAergic and glycinergic neurons are present throughout the brainstem respiratory network where they play a prominent role in inspiratory pattern generation (Paton and Richter 1995b; Ramirez et al., 1996; Shao and Feldman 1997; Tryba et al., 2003). Although inspiratory rhythm persists in the absence of GABAergic and glycinergic transmission, $GABA_A$ and GlyR blockade significantly disrupt inspiratory rhythm *in vivo* and *in vitro* in multiple ways, such as changing inspiratory burst frequency and inducing seizure-like bursting and tonic firing (Ramirez et al., 1996; Pierrefiche et al., 1998; Busselberg et al., 2001). Within the respiratory network, GABA and glycine serve multiple functions. In the Bötzinger Complex, which is located rostral to the PBC (Figure 1.2), GABAergic and glycinergic expiratory neurons fire during expiration and mediate expiratory-phase inhibition. Inspiratory GABAergic neurons (Kuwana et al., 2006) and GlyR immunoreactive (Liu and Wong-Riley 2002) neurons are also found in the PBC, where inhibitory synaptic transmission is thought to regulate excitability by providing tonic inhibition during inspiratory activity (Johnson et al., 2001). Further caudally in the respiratory network, premotor GABAergic and glycinergic neurons project to the XII nucleus (Li et al., 1997), which also contains inhibitory interneurons. Some of these GABAergic and/or glycinergic neurons may be the source of the inspiratory-phase inhibitory synaptic inputs that HMs receive and that have been shown to shape the pattern of HM inspiratory-phase activity (Saywell and Feldman 2004). Given the importance of inhibitory synaptic transmission in shaping the pattern of inspiratory-phase discharge and in generating synchronous oscillations in other brain

regions, I investigated the role of GABA and glycine in synchronizing inspiratory-phase activity on a shorter time scale.

Previous work from our laboratory has shown that GABAergic and glycinergic transmission are important in generating synchronous oscillations recorded from motor nerves of the neonatal brainstem respiratory network (Bou-Flores and Berger 2001). In the present study, I extended this work by examining inspiratory-phase synchronous oscillations during postnatal development. In particular, I recorded inspiratory-phase activity from XII nerves of neonatal and juvenile mice in order to measure synchronous oscillation frequency and to examine the role of GABA and glycine in generating oscillations. To further probe the mechanisms by which oscillations are produced, I investigated how oscillation frequency is modulated by prolonging the time course of GABAergic inhibition.

Methods

Slice Preparations

In vitro experiments were performed on either the rhythmically active (Figure 2.1) or the non-rhythmically active medullary slice preparations from Swiss-Webster mice (P0-11). For experiments in which I measured oscillation frequency over postnatal development (Figure 2.2), I used P0-11 mice. However, in all other figures, I divided the mice into two age groups: neonates (P0-6) and juveniles (P7-10) to divide the sample population into the first and second weeks of postnatal development, respectively. Mice were anesthetized with halothane and sacrificed by decapitation in accordance with the regulations of the University of Washington Institutional Animal Care and Use Committee (IACUC).

Methods used in dissecting the rhythmically active medullary slice preparation have been described previously (Funk et al., 1993). In brief, the medulla and cervical spinal cord were isolated and removed from the mouse. The brainstem and spinal cord were pinned onto a Sylgard® block and the block was mounted into a vibratome platform (Pelco 101 Series 1000, Redding, CA). Brainstem slices were then cut from rostral to caudal. After the facial nucleus was no longer visible, another 200 μm slice was cut prior to cutting the rhythmic slice. The thickness of the rhythmic slice was increased from 500-700 μm according to the age of mouse. Slices from younger mice were thinner than those obtained from older mice. This slice was placed into the recording chamber and superfused for at least 20 minutes with 8 mM K^+ ACSF before recording began.

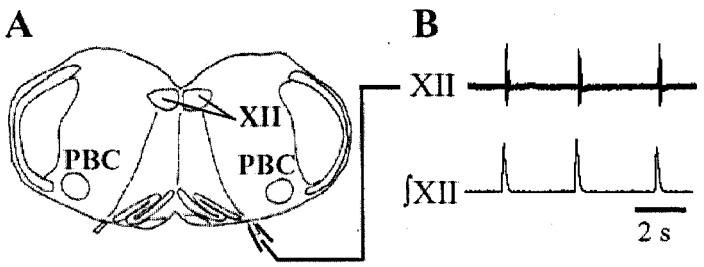

Figure 2.1. Mouse rhythmically active medullary slice preparation. A. This slice preparation contains inspiratory rhythm generating neurons in the PreBötzinger Complex (PBC) that transmit inspiratory-phase activity, possibly through a premotor area, to motoneurons of the hypoglossal nucleus (XII). Hypoglossal nerve roots exit the ventral surface of the brainstem slice and exhibit inspiratory-phase activity (B, top trace). Raw hypoglossal nerve root recordings are rectified and integrated (B, bottom trace).

For studies utilizing the non-rhythmically active medullary slice preparation, the brainstem was removed and 300 μm slices containing the XII motor nucleus were cut. Slices were incubated for 1h at 37°C prior to recording.

Recording

For the rhythmically active slice preparation, the temperature of the custom-made recording chamber was maintained between 27 and 28°C. Glass suction electrodes were pulled from borosilicate glass and filled with ACSF to record from the cut ends of XII rootlets. Raw nerve signals were amplified and AC filtered at 0.1 Hz using CyberAmp 320 and pClamp8 (Axon Instruments, Union City, CA) and the signal was sampled at 5kHz. To measure integrated nerve activity, the filtered signal was rectified and integrated using a custom built "leaky" integrator with a time constant of 100 ms.

Whole-cell voltage-clamp recordings were made from HMs in non-rhythmically active medullary slices visualized using IR-DIC microscopy (Zeiss, Inc.) and camera (Hamamatsu Co.). Cells were voltage-clamped at a holding potential of –70 mV (after correction for the measured liquid junction potential of 10 mV) using an Axopatch 200B amplifier (Axon Instruments). Recording electrodes were pulled from borosilicate glass and had a resistance of 3-3.5 MΩ. Access resistance (R_a) was monitored periodically during the recording and recordings were rejected if R_a was more than 30 MΩ, or changed by more than 25% during the recording. Whole-cell current was A-D converted at 20kHz using pClamp8 (Axon Instruments) after low-pass filtering at 5 kHz with an 8-pole Bessel filter.

Solutions and Drug Application

The normal ACSF used for rhythmically active slice preparations contained (in mM): 118 NaCl, 3 KCl, 1 $MgCl_2$, 1 NaH_2PO_4, 25 $NaHCO_3$, 30 D-glucose and 1.5 $CaCl_2$. The osmolarity of the ACSF was 300 mOsm and the ACSF was pH adjusted to 7.4 with

NaOH. For recording spontaneous rhythmic activity, the same ACSF was used except that KCl concentration was elevated to 8 mM KCl. ACSF was superfused over the preparation at 2-3 ml/min and recycled using a peristaltic pump (Rainin). The ACSF used for non-rhythmically active medullary slice preparations contained (in mM): 119 NaCl, 2.5 KCl, 1.3 $MgSO_4$, 1 NaH_2PO_4, 26.2 $NaHCO_3$, 11 D-glucose and 2.5 $CaCl_2$. During dissection, slicing and recording, both ACSFs were gassed with 95% O_2 and 5% CO_2. The internal solution for whole cell voltage clamp recordings contained (in mM): 140 CsCl, 1 $CaCl_2$, 3.45 Cs-BAPTA, 5 Mg_2-ATP, 10 HEPES and 10 QX-314 (pH = 7.3 with CsOH; osmolarity = 290 mOsm).

All drugs were bath applied in the ACSF and washed in or out for at 10-15 minutes prior to recording inspiratory activity in drug condition or washout, respectively. In experiments to block $GABA_A$ and GlyRs, SR95531 (0.5 μM, Sigma) and strychnine hydrochloride (1 μM, Sigma), respectively, were applied for 10 minutes prior to recording. Zolpidem (0.1 μM – 0.5 μM, Sigma) prepared from a 50 mM stock solution in ethanol was diluted to the desired concentration in bath solution just prior to the start of the experiment. Substance P (0.05 μM, Sigma) was bath applied to increase the excitability of the slice (Gray et al., 1999; Yasuda et al., 2001). In whole cell recordings of GABAergic mIPSCs, the bath solution contained DNQX (10 μM, RBI), AP5 (25 μM, Tocris), TTX (1 μM, Alomone Labs) and strychnine hydrochloride (1 μM). Bicuculline methodide (5 μM, Sigma) was bath applied at the end of some whole cell experiments to confirm the GABAergic nature of mIPSCs.

Data Analysis

Inspiratory bursts were selected in Clampfit (Axon Instruments) and analyzed in Igor Pro (Wavemetrics, Inc) using a routine developed by Dr. Randy K. Powers. For each recording condition, 15-20 inspiratory bursts were selected and used to create 15-20 absolute power spectra in which the frequency resolution was 1 Hz. Average absolute power spectra were computed by averaging the 15-20 absolute power spectra for each condition. Average relative power spectra were calculated from the average absolute power spectra by dividing the absolute power at each data point (0-99 Hz) by the absolute power for all data points (0-99 Hz). For Figure 2.2, oscillation frequency was measured by finding the frequency of the dominant peak in the average relative power spectrum. The dominant peak was defined as the largest peak in the average relative power spectrum, not including the power at low frequencies (0-5 Hz) that is due to the overall envelope of the inspiratory burst. Only average relative power spectra of control recordings were used to find oscillation frequency. A least-squares regression line was used to fit and determine the statistical significance of the change in oscillation frequency of the dominant peak over postnatal age. Unpaired t-tests were used to compare oscillation frequencies recorded from neonate and juveniles slices.

To measure relative power of synchronous oscillations, as opposed to measuring synchronous oscillation frequency, each average relative power spectrum was binned (10 Hz bin width). To bin the relative power within each average relative power spectrum, I located the dominant peak in the average relative power spectrum. The location of this peak and its concomitant 10 Hz bin defined the starting point of the binning process whereby all other bins were in 10 Hz increments above and below this starting bin. Then, I was able to compute the fraction of relative power within the 10 Hz

bin that contained the dominant peak. To do this, I added all points within each 10 Hz bin and divided that number by the total relative power from 0-99 Hz. By comparing these fractions of relative power, I measured changes in the relative power of synchronous oscillations following various pharmacological manipulations. Paired t-tests were used to compare changes in relative power between control and drug conditions.

Peak integrated activity and burst duration were measured in Igor Pro using the rectified and integrated traces of the inspiratory bursts. Peak integrated activity was the highest point of the rectified and integrated traces. Burst duration was defined as the time at 95% of the integrated area subtracted by time at 5% of the integrated area. Peak integrated activity and burst duration values were computed for the same 15-20 inspiratory bursts used for power spectral analysis. The average peak integrated activity and burst duration were compared across recording conditions. Paired t-tests were used to determine statistical significance of changes in peak integrated activity, inspiratory burst duration and inspiratory burst frequency, separately, between control and drug conditions.

Event detection and off-line analysis of the recorded spontaneous miniature GABAergic IPSCs (mIPSCs) was performed using the MiniAnalysis 5.6 software program (Synaptosoft, Decatur, GA). We determined the peak amplitude and decay time (measured as the time for the mIPSC to decay to 37% of its peak value) of all individual events whose amplitude exceeded the detection threshold (set manually by visual inspection of the data traces). Event detection was started after a minimum pre-equilibration period of 5 minutes in each bath solution and 1-4 minute long recorded segments during perfusion with control solution and after adding Zolpidem were

selected for automated event detection. Overlapping events or events with slow rise times (>10 ms) were excluded from analysis by visual inspection of the detected mIPSCs. Miniature event frequency varied considerably from cell-to-cell, but a minimum of 35 events was used per cell to calculate average values for mIPSC amplitude and decay time in individual cells. Only one cell per slice was tested and only one concentration of Zolpidem (0.1, 0.2, or 0.5 microM) was tested per cell. Statistical significance was determined with the paired and unpaired t-tests within and between cell groups and with the Kolmogorov-Smirnov test for comparisons within individual cells. Significance was set at $p < 0.05$.

To investigate the effect of zolpidem on oscillation frequency, I computed the average relative power spectrum, as described above, for the control condition, following bath application of strychnine and subsequent bath application of strychnine and zolpidem. For each average relative power spectrum, I determined the oscillation frequency by computing the median oscillation frequency within the 9-59 Hz frequency range (Igor Pro). To calculate median oscillation frequency, I added all the relative power values between 9-59 Hz and computed the oscillation frequency that divided the relative power into two equal sums. Statistical significance was determined using paired t-tests.

Results

Oscillation Frequency Increases over Postnatal Development

I found that oscillation frequency gradually increases over postnatal development and spanned a range of frequencies, from 6 to 57 Hz, in P0-11 mouse slices. Figure 2.2A shows inspiratory bursts from P0 and P10 mouse slices acquired

from XII nerve recordings. The clusters of action potentials are evident in both neonatal and juvenile slices. Using power spectral analysis, I measured the oscillation frequency by determining the frequency at which the dominant peak occurred in the average power spectrum (Figure 2.2B). This method of determining oscillation frequency is rooted in classical work that investigated inspiratory-phase synchronous oscillations (Richardson and Mitchell 1982; Cohen et al., 1987). The dominant peak of the average power spectrum occurred at a higher frequency in juvenile mouse slices than in neonatal mouse slices. In Figure 2.2C, the plot of oscillation frequency versus postnatal day for 52 slices shows that oscillation frequency significantly increased from 8 to 41 Hz with postnatal development ($y = 3x + 8$, $r^2 = 0.62$, $p < 0.01$). I also categorized the same oscillation frequency measurements into data acquired from neonate (P0-6) and juvenile (P7-11) age groups and calculated mean oscillation frequency for each age group. I found that mean oscillation frequency increased from 17 ± 12 Hz ($n = 15$) in neonates to 38 ± 7 ($n = 37$) in juveniles ($p<0.0001$, unpaired t-test).

I measured mean inspiratory burst duration and mean inspiratory burst frequency in neonates (P0-6) and juveniles (P8-10) and found that these parameters do not change with postnatal development. The mean inspiratory burst duration was 522 ± 24 ms ($n = 17$), in neonates, and 491 ± 10 ms ($n = 35$), in juveniles (unpaired t-test, $p = 0.15$). The mean inspiratory burst frequency was unchanged in both neonates (0.08 ± 0.01 Hz, $n = 17$) and in juveniles (0.08 ± 0.01 Hz, $n = 35$) (unpaired t-test, $p = 0.97$).

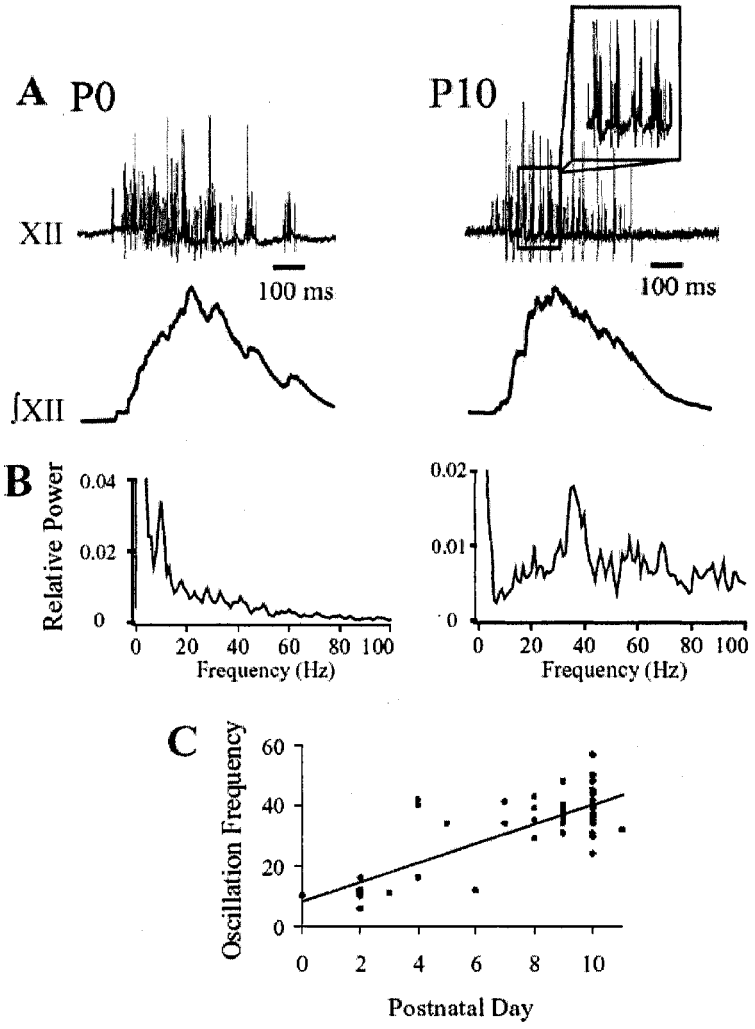

Figure 2.2. Oscillation frequency increases over postnatal development. A. Hypoglossal nerve recordings of inspiratory bursts from P0 and P10 mouse slices. Within each inspiratory burst, the clusters of action potentials that occur at regular intervals are called synchronous oscillations. In the inset, part of the inspiratory burst recorded from the P10 slice is shown on an expanded time scale (approximately 2x) to better display the synchronous oscillations. B. We measured the frequency and relative power of synchronous oscillations by computing the average relative power spectra for the P0 and P10 slices. Note that the dominant peak in the average relative power spectrum occurs at 10 Hz in the P0 slice, while the dominant peak occurs at 36 Hz in the P10 slice. C. The frequency of the peak in the power spectra increases over postnatal development from 8 to 41 Hz in P0-11 mice ($y = 3x + 8$, $r^2 = 0.62$, $p < 0.01$). Data from 52 slices are pooled and plotted.

GABAergic and Glycinergic Transmission Contribute to Motoneuron Synchronization

In each experiment, I recorded inspiratory-phase activity from a XII rootlet in control ACSF. Next, strychnine, a GlyR antagonist, or SR95531, a $GABA_AR$ antagonist, was bath applied separately, and then both antagonists were bath applied together. I used SR95531 because it is a more specific $GABA_AR$ antagonist than bicuculline methiodide which also blocks small-conductance Ca^{2+} activated potassium channels (Khawaled et al., 1999). The antagonists were washed out for at least 20 minutes prior to recording XII nerve rootlet activity in the wash condition. In Figure 2.3A, representative inspiratory bursts recorded from a P0 mouse slice in control, 1 μM strychnine, 1 μM strychnine and 0.5 μM SR95531, and wash conditions are shown. Using the P0 slice recording shown in Figure 2.3A, the power spectra of 20 different inspiratory bursts were averaged for each of the four conditions and the average power spectra are shown in Figure 2.3B.

In Figure 2.3B, the 8-17 Hz frequency bins contain the dominant peaks for the average power spectra. The fraction of relative power within the 8-17 Hz frequency bins is reduced following strychnine bath application compared to control. Following combined strychnine and SR95531 bath application, the fraction of relative power within the same 8-17 Hz frequency bin is further reduced. This reduction in relative power is reflected in the average power spectra (Figure 2.3B, inset) as the lack of a dominant peak when both $GABA_A$ and GlyRs are blocked. The return of the dominant peak during wash demonstrates the partial reversibility of this reduction in oscillation power. During wash, oscillation power in the average power spectrum is similar to that following bath application of strychnine (Figure 2.3B, inset). This suggests that strychnine does not wash out. In Figure 2.3C, the average power spectra for a similar

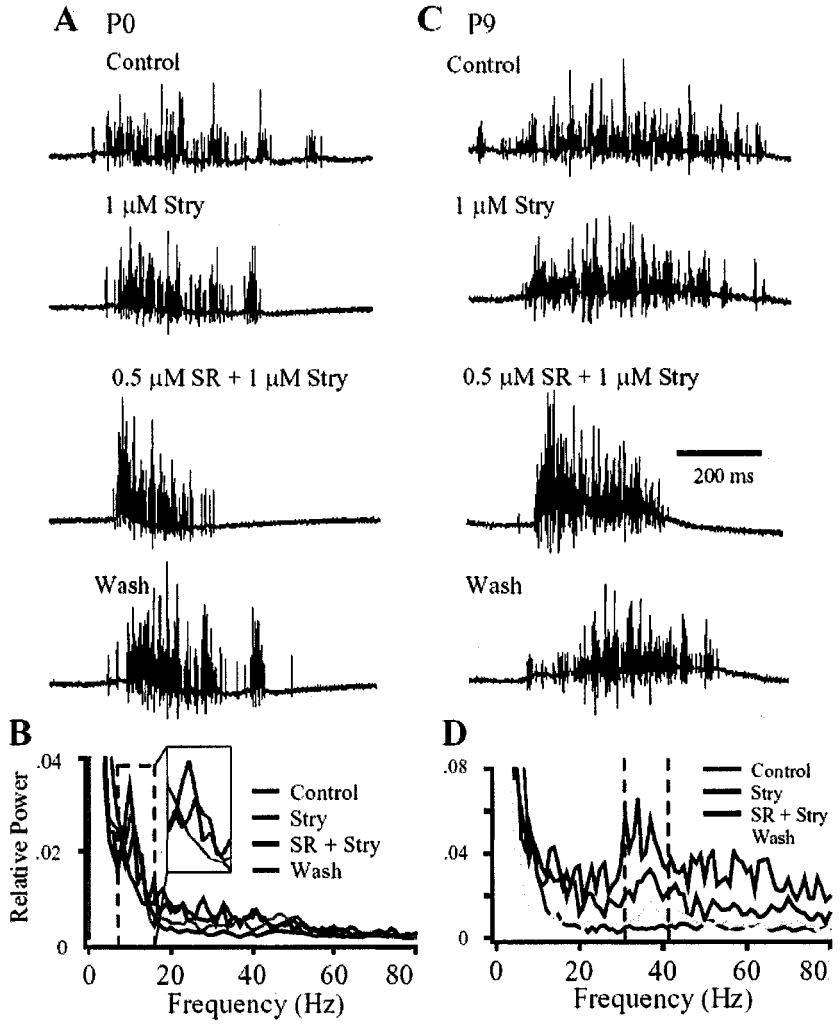

Figure 2.3. GABAergic and glycinergic transmission are required to generate robust synchronous oscillations in neonatal and juvenile mouse slices. A. Representative inspiratory bursts recorded from a P0 slice in control solution, following styrchnine (Stry) bath application, Stry and SR95531 (SR) bath application and during wash. Clusters of action potentials are present in control, but are not found when $GABA_A$ and GlyRs are blocked. B. Average power spectra for the P0 slice shown in (A). Dashed lines indicate the boundaries of the 8-17 Hz frequency bins containing the dominant peaks in all average power spectra. Inset shows the average power spectra within the 8-17 Hz frequency bin. Relative power within this frequency bin is reduced following Stry application and is diminished in the presence of 1 μM Stry and 0.5 μM SR. The dominant peak returns toward control during wash. Power spectra were computed by averaging 20 inspiratory bursts for each condition. C. Representative inspiratory bursts recorded from a P9 slice in control solution, following bath application of Stry, Stry and SR and following wash. D. Average power spectra for the P9 slice shown in (C). Dashed lines indicate the boundaries of the 32-41 Hz frequency bins containing the dominant peaks in all average power spectra. Relative power within the 32-41 Hz bin decreased following Stry bath application and in the presence of Stry and SR. Time calibration bar in C applies to all traces in A and C.

experiment in a P9 mouse are shown. Relative power in the frequency bins containing the dominant peaks (32-41 Hz) is reduced following GlyR blockade and relative power is further reduced following $GABA_A$ and GlyR blockade. The lack of a dominant peak in the average power spectrum during $GABA_A$ and GlyR blockade (Figure 2.3D) reflects this reduction in relative power. The dominant peak partially returns following washout of $GABA_A$ and GlyR antagonists.

Summary data demonstrating the role of GABAergic and glycinergic transmission in synchronizing HM activity over postnatal development are shown in Figure 2.4. In neonatal mouse slices, bath application of strychnine alone decreased oscillation power by -21 ± 7 % (n = 7, $p < 0.05$) and bath application of SR95531 alone decreased oscillation power by -39 ± 11 % (n = 6, $p < 0.05$) compared to control. Bath application of strychnine and SR95551 together in neonates decreased oscillation power by -49 ± 7 % (n = 10, $p < 0.0001$) compared to control and this effect was partially reversed following wash (-23 ± 12 %, n = 13, n.s.). In juveniles (P7-10),

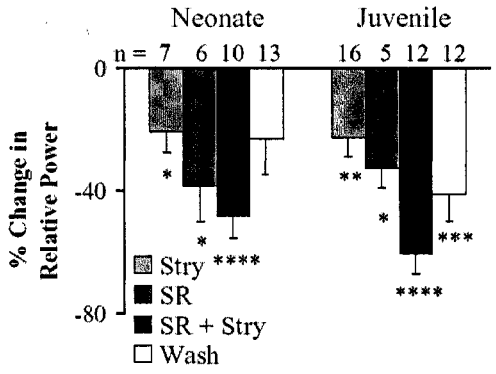

Figure 2.4. Summary of the effects of $GABA_A$ and GlyR blockade on relative power of synchronous oscillations. In neonates and juveniles, bath application of Stry or SR, separately, and bath application of Stry and SR, together, reduce oscillation power. The reduction is oscillation power is partially reversed. Mean ± SE. (*, $p < 0.05$; **, $p < 0.01$; ***, $p < 0.001$; ****, $p < 0.0001$; paired t-test vs. control)

GlyR blockade alone reduced oscillation power by -20 ± 7 % ($n = 14$, $p < 0.01$) and bath application of SR95531 alone decreased oscillation power by 33 ± 6 % ($n = 5$, $p < 0.05$). Bath application of $GABA_A$ and GlyR antagonists together decreased oscillation power by 61 ± 6 % ($n = 12$, $p < 0.0001$), and this effect was partially reversible (-41 ± 9 %, $n = 12$, $p < 0.001$).

The effect of $GABA_A$ and GlyR blockade on synchronous oscillations was also apparent in the recording of the rectified and integrated XII nerve traces, representative examples of this are shown in Figure 2.5A and B. In a P0 slice (Figure 2.5A), the control trace (black trace) shows a 10 Hz oscillation within the inspiratory burst that is abolished following $GABA_A$ and GlyR blockade (red trace), and returns in the wash condition (gray trace). In a P10 slice (Figure 2.5B), oscillation frequency in control (black trace) is higher, at 34 Hz, and this oscillation is less prominent in the rectified and integrated trace following $GABA_A$ and GlyR blockade (red trace).

Blocking GABAergic and Glycinergic Transmission Increases Slice Excitability

Blocking $GABA_A$ and GlyRs increased slice excitability for both neonate and juvenile mice. I measured changes in peak integrated activity, inspiratory burst duration, and inspiratory burst frequency relative to control for neonates and juveniles. In neonates (Figure 2.5A and C1), bath application of SR95531 or strychnine, separately, increased mean peak integrated activity (SR95531: 36 ± 9 %, $n = 8$, $p < 0.01$; strychnine: 36 ± 5 %, $n = 10$, $p < 0.01$). Bath application of SR95531 and strychnine together further increased mean peak integrated activity (103 ± 17 %, $n = 18$, $p < 0.0001$) and this effect was partially reversed following wash (65 ± 10 %, $n = 18$, $p < 0.01$). In Figure 2.5A, the rectified and integrated traces of inspiratory bursts for a

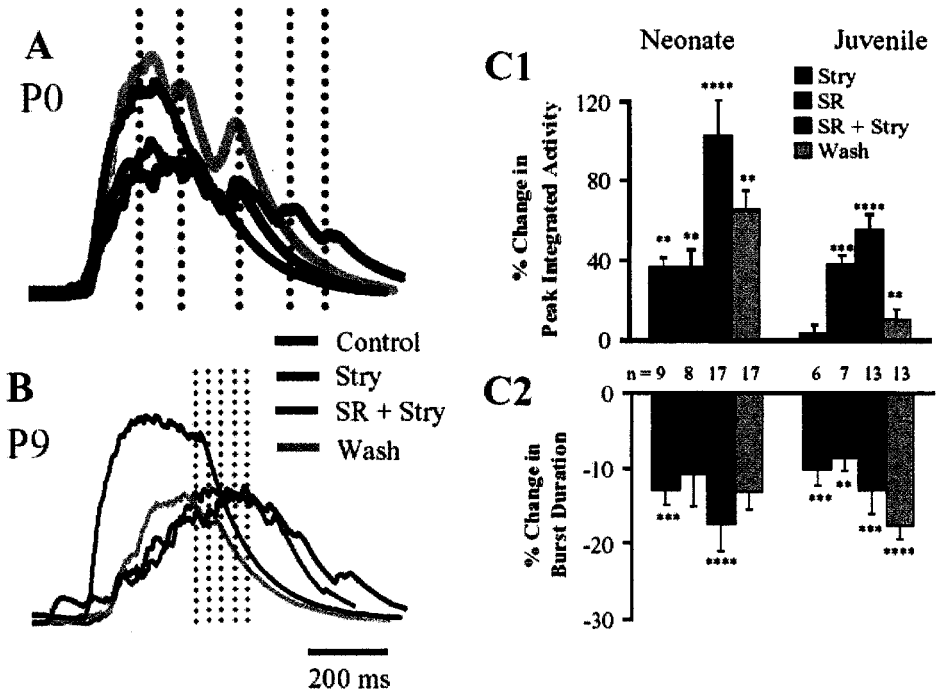

Figure 2.5. $GABA_A$ and GlyR blockade increased peak integrated hypoglossal nerve activity and decreased inspiratory burst duration in neonates and juveniles. A. Representative rectified and integrated traces from a P0 slice show that with Stry bath application peak integrated activity increased and with subsequent combined SR and Stry bath application it increased further. Dashed lines in (A) and (B) are aligned with synchronous oscillation peaks in the control traces. B. Representative rectified and integrated hypoglossal nerve traces from a P9 slice show that peak integrated activity did not change with Stry bath application, but increased with subsequent SR and Stry bath application. Washing reversed this effect. C1. Peak integrated hypoglossal nerve activity increased with Stry application alone in neonates, but not in juveniles. Bath application of SR increased peak integrated activity in both age groups as did bath application of both SR and Stry. This effect was partially reversed following wash. C2. Blockade of GlyRs, separately, or $GABA_A$ and GlyRs, together, decreased inspiratory burst duration in neonates. In juveniles, blockade of $GABA_A$ and GlyRs, separately and together, decreased inspiratory burst duration. Mean ± SE. (**, $p < 0.01$; ***, $p < 0.001$; ****, $p < 0.0001$; paired t-test vs. control)

single neonatal mouse show the increase in peak integrated activity following antagonist application. Following strychnine bath application (blue trace), peak integrated activity increased compared to control (black trace) and increased further when $GABA_A$ and GlyRs were blocked together (red trace). In juveniles, bath application of strychnine alone did not affect peak integrated activity (Figure 2.5C1). In the same age group, bath application of SR95531, separately, and both antagonists together increased peak integrated activity (SR95531: 38 ± 5 %, $n = 7$, $p < 0.001$,

SR95531 and strychnine: 55 ± 8 %, n = 13, $p < 0.0001$) and this effect was partially reversible (10 ± 5 %, n = 13, $p < 0.01$) (Figure 2.5C1). In Figure 2.5B, the rectified and integrated traces show the increase in peak integrated activity in a juvenile mouse following combined $GABA_A$ and GlyR blockade (red trace) compared to control (black trace).

I also measured the effect of $GABA_A$ and GlyR antagonists on mean inspiratory burst duration in neonates and juveniles (Figure 2.5C2). In neonates, bath application of strychnine (-13 ± 2 %, n = 10, $p < 0.001$), but not SR95531 (-11 ± 4 %, n=8, $p = 0.12$), decreased mean burst duration. When SR95531 and strychnine were bath applied together, mean burst duration decreased (-17 ± 4 %, n = 18, $p < 0.001$) and this effect was not reversed (-13 ± 2 %, n = 18, $p < 0.0001$). In juveniles, bath application of SR95531 or strychnine, separately, decreased mean burst duration (SR95531: -9 ± 2 %, n=8, $p < 0.01$; strychnine: -10 ± 2 %, n = 6, $p < 0.001$). Bath application of SR95531 and strychnine together decreased mean burst duration (-13 ± 3 %, n = 13, $p < 0.001$) and this effect was not reversible by wash (18 ± 2 %, n = 13, $p < 0.0001$). The decrease in burst duration, in neonates and juveniles, is reflected in the rectified and integrated traces shown in Figure 2.5A and B. GlyR blockade (blue traces) and combined $GABA_A$ and GlyR blockade (red traces) reduced mean burst duration in the P0 and P9 slices compared to control (black traces).

Bath application of $GABA_A$ and GlyR antagonists changed the pattern of respiratory rhythm in neonates and juveniles. Following $GABA_A$ and GlyR blockade, the XII nerve output occasionally exhibited seizure-like activity. It was difficult to consistently measure the inspiratory burst frequency during these seizure-like events, because the bursts often merged into one long burst as the antagonists washed into the

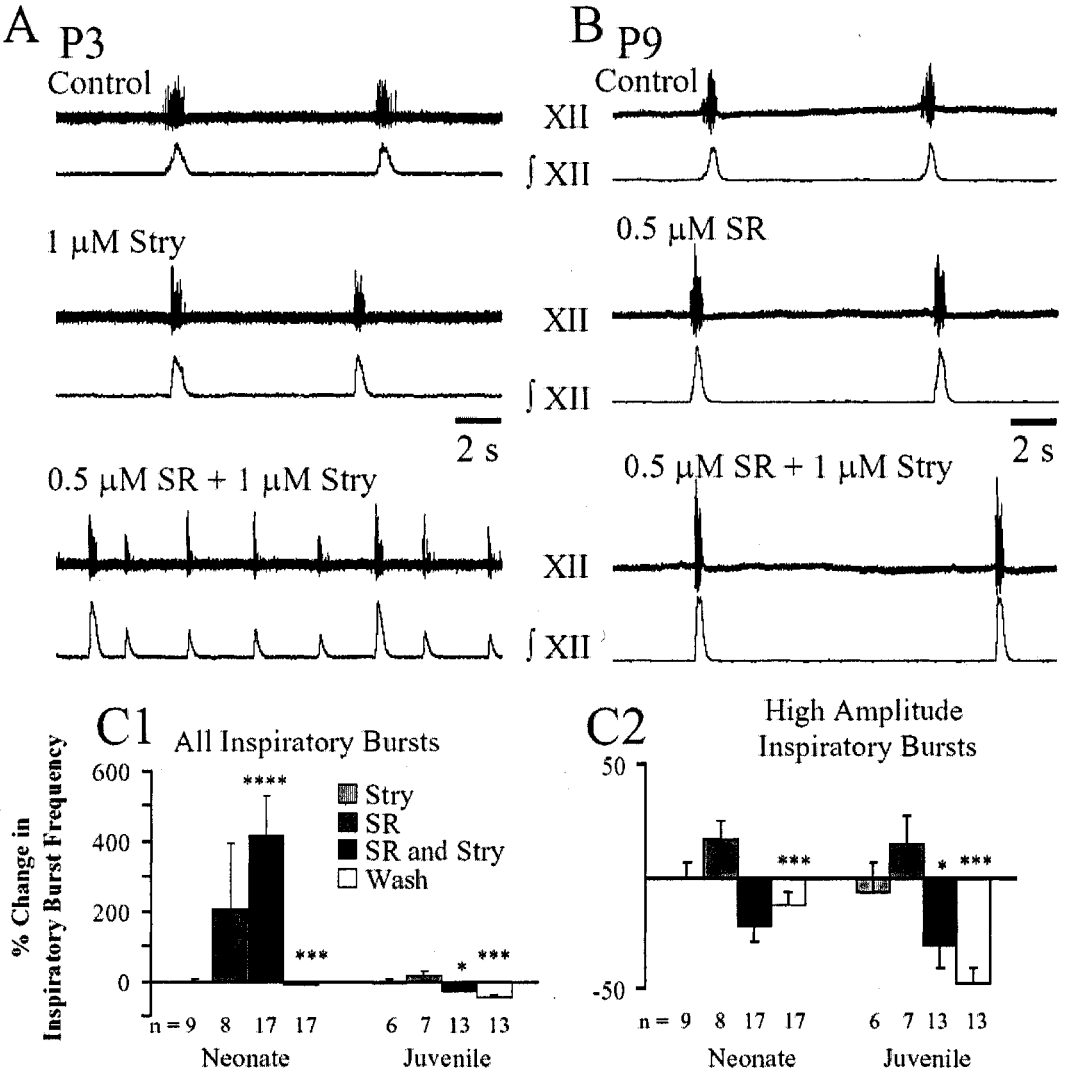

Figure 2.6. $GABA_A$ and GlyR blockade induced a secondary rhythm in neonates, but not in juveniles. A. Representative hypoglossal nerve recordings from a P3 slice in control condition, following bath application of Stry and following bath application of SR and Stry. For each condition, the top trace is a raw hypoglossal nerve recording and the bottom trace is the corresponding rectified and integrated trace. $GABA_A$ and GlyRs blockade induced a secondary inspiratory rhythm composed of lower amplitude and higher frequency inspiratory bursts. B. Representative hypoglossal nerve recordings from a P9 slice in control condition, following bath application of SR alone and combined bath application of SR and Stry. Although peak integrated activity increased following $GABA_A$ and GlyR blockade, inspiratory burst frequency did not change. C1. Percent change in mean inspiratory burst frequency relative to control when all inspiratory bursts are counted. Inspiratory burst frequency increased following $GABA_A$ and GlyR blockade in neonates, but not in juveniles. The legend in C1 applies to C1 and C2. C2. Percent change in mean inspiratory burst frequency relative to control when only high amplitude bursts are counted. Following $GABA_A$ and GlyR blockade, inspiratory burst frequency did not change in neonates, but decreased in juveniles ($p < 0.05$). Mean ± SE. (*, $p < 0.05$; ***, $p < 0.0001$)

slice. For this reason, mean inspiratory burst frequency was measured in blocks of activity that did not include seizure-like activity.

Neonate and juvenile slices in control conditions exhibited a primary rhythm composed only of large amplitude bursts that occurred at a relatively low frequency (Figure 2.6A and B, respectively). This primary rhythm persisted, in both age groups, following separate blockade of $GABA_A$ or GlyRs (Figure 2.6A and B). Subsequent combined $GABA_A$ and GlyR blockade gave rise to a secondary rhythm, in neonates (Figure 2.6A) but not in juveniles (Figure 2.6B). The secondary rhythm consisted of low amplitude inspiratory bursts occurring at a higher burst frequency than the inspiratory bursts of the primary rhythm (Figure 2.6A).

For all recordings, I used only the high amplitude inspiratory bursts for power spectral analysis. Due to the two inspiratory rhythms exhibited by neonatal slices following $GABA_A$ and GlyR blockade, I approached mean inspiratory burst frequency analysis, for all conditions and both age groups, in two ways. First, I included all inspiratory bursts, those in the primary and secondary rhythm, in measuring inspiratory burst frequency; these data are summarized in Figure 2.6C1. Second, I counted only the high amplitude bursts; these data are summarized in Figure 2.6C2.

First, I report the effects of $GABA_A$ and GlyR blockade on inspiratory burst frequency measured from neonatal slices. When all inspiratory bursts were counted (Figure 2.6C1), GlyR blockade did not affect mean inspiratory burst frequency (0 ± 7 %, n=9, n.s.). $GABA_AR$ blockade alone substantially increased inspiratory burst frequency in a single P2 slice out of 8 neonatal slices studied by giving rise to a secondary inspiratory rhythm. This result increased the variability of the data points and when all inspiratory bursts were counted, $GABA_AR$ blockade did not significantly effect mean

inspiratory burst frequency in neonates (204 ± 190 %, n = 8, n.s.). When counting all inspiratory bursts, I found that combined $GABA_A$ and GlyR blockade increased mean inspiratory burst frequency in neonates (415 ± 114 %, n = 17, $p < 0.001$). This effect was reversible during wash (-13 ± 6 %, n = 17, $p < 0.001$).

In neonatal slices, when only high amplitude bursts were counted (Figure 2.6C2), GlyR blockade alone did not effect inspiratory burst frequency. As GlyR blockade alone did not induce a secondary rhythm, both forms of analysis yielded the same result as reported above. $GABA_AR$ blockade alone (17 ± 8 %, n = 8, n.s.) and combined $GABA_A$ and GlyR blockade (22 ± 7 %, n = 17, n.s.) did not affect inspiratory burst frequency in neonates. Inspiratory burst frequency decreased during wash (-13 ± 6 %, n = 17, $p < 0.001$).

In juveniles, $GABA_A$ and GlyR blockade did not yield a secondary rhythm therefore both forms of analysis yielded the same result (Figure 2.6C1 and C2). GlyR or $GABA_AR$ blockade, separately, did not affect mean inspiratory burst frequency (-7 ± 14 %, n = 6, n.s. and 14 ± 13 %, n = 7, n.s., respectively). Bath application of the same concentrations of strychnine and SR95531 as used on neonatal slices decreased inspiratory burst frequency (-31 ± 10 %, n = 13, $p< 0.05$) in juveniles and inspiratory burst frequency did not recover following wash (48 ± 8 %, n = 13, $p < 0.001$).

Overall, $GABA_A$ and GlyR blockade increases slice excitability in neonates and juveniles by increasing mean peak integrated activity. However, mean inspiratory burst frequency showed an age dependent sensitivity to $GABA_A$ and GlyR blockade in that bath application of $GABA_A$ and GlyR antagonists together induced a secondary rhythm in neonates, but not in juveniles.

Increasing Excitability by Substance P Does Not Result in a Decrease in Oscillation Power

I have shown that blocking inhibitory synaptic transmission decreases the power of synchronous oscillations while it increases the excitability of the slice, that is, there is an increase in peak integrated XII nerve activity. Although GABAergic and glycinergic transmission are likely involved in synchronizing motoneuron activity, it is possible that any intervention that increases slice excitability and therefore increases nerve activity will reduce the power of the oscillations. The oscillations are characterized by clusters of action potentials within a burst that are separated by short periods of little or no activity. Increasing excitability may reduce oscillation power by filling in the gaps between the clusters of action potentials. If this interpretation of the data is true, increasing the excitability using another method should also decrease oscillation power.

To test this hypothesis, I increased slice excitability by bath applying 0.05 – 0.1 μM Substance P to rhythmically active slices from juvenile mice (P8-10). Substance P increases HM excitability by inhibiting the TASK-1 K^+ channel (Talley et al., 2000). Extensive studies that investigated the effects of Substance P on respiratory rhythm have shown that local application of Substance P in the PBC (Gray et al., 1999) or XII nucleus (Yasuda et al., 2001) increase inspiratory burst frequency and inspiratory burst amplitude. I bath applied Substance P to examine whether increasing slice excitability also reduces oscillation power.

As expected, Figure 2.7A shows that bath application of 0.05 - 0.1 μM Substance P elevated the activity recorded from XII nerve roots by increasing mean peak integrated activity (Figure 2.7B: 123 ± 55%, n=12, $p<0.05$) and this effect was reversed by wash (Figure 2.7A and B: 5 ± 33%, n=10, n.s.). Substance P bath

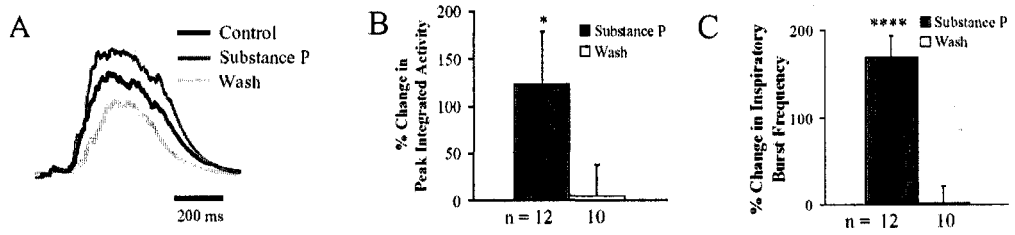

Figure 2.7. Bath application of 0.05 - 0.1 μM Substance P increased slice excitability. A. Representative rectified and integrated traces show that peak integrated activity increased with Substance P (0.05 μM) and this effect is reversible. B. Bath application of Substance P increased mean peak integrated activity (123 ± 55%, $p < 0.05$) and washing reversed this effect (5 ± 33%, n.s.). C. Bath application of Substance P increased mean inspiratory burst frequency (170 ± 24%, $p < 0.0001$) and this effect was reversed in wash (3 ± 19%, n.s.).

application also increased mean inspiratory burst frequency (Figure 2.7C: 170 ± 24%, n=12, $p<0.0001$) from 0.07 ± 0.03 Hz in control to 0.18 ± 0.05 Hz in Substance P. Mean inspiratory burst frequency returned to 0.07 ± 0.05 Hz following wash (Figure 2.7C: 3 ± 19%, n=10, n.s.). Unlike the $GABA_A$ and GlyR antagonists, Substance P increased mean burst duration (7 ± 3%, n=12, $p < 0.05$) and this effect was reversible (5 ± 3%, n=10, n.s.).

In contrast to the results seen with $GABA_A$ and GlyR blockade, the increase in slice excitability is not accompanied by a decrease in oscillation power. Examples of inspiratory bursts recorded from two different slices in control solution, following 0.05 μM Substance P application, and in wash are shown in Figure 2.8A and C. In the slice shown on the left, the relative power of the oscillation in the 35 to 44 Hz bin increases following bath application of 0.05 μM Substance P and oscillation power is diminished during wash (Figure 2.8B). A similar increase in oscillation power was observed in 6 out of 8 cells tested (100 ± 41%, $p < 0.05$). In the slice shown on the right, relative power in the 33 to 42 Hz bins does not change following Substance P application

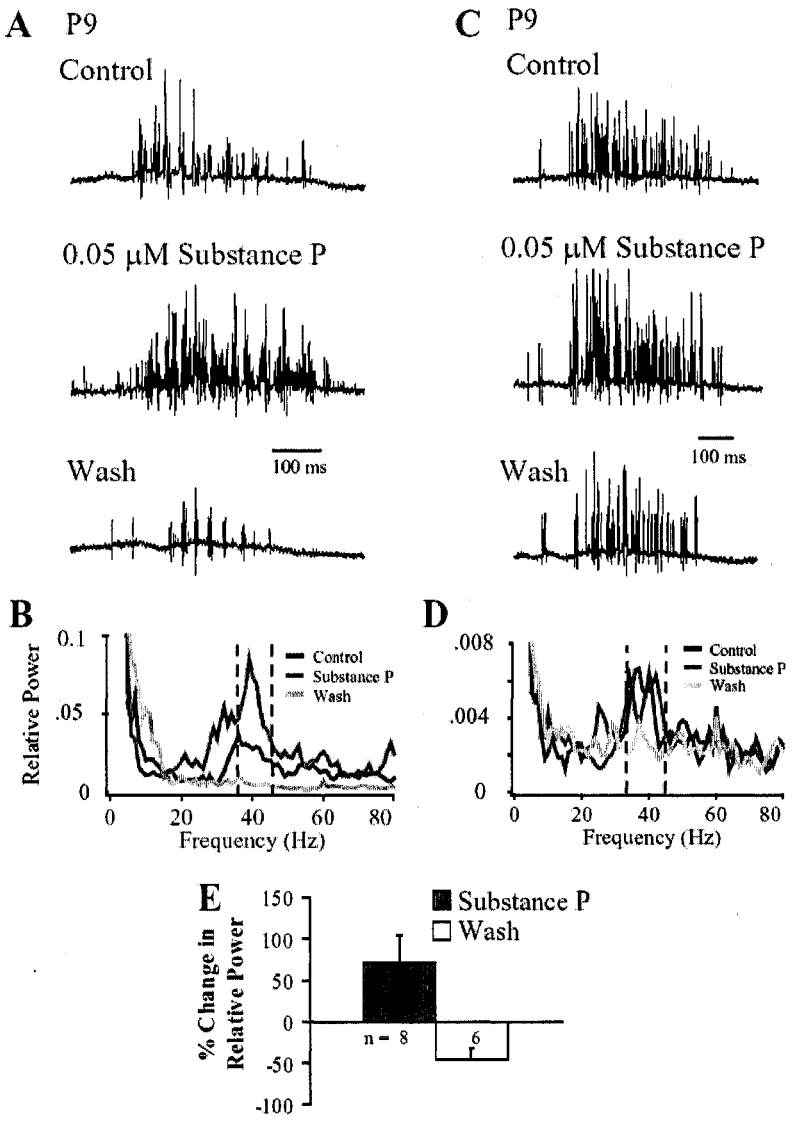

Figure 2.8. Substance P does not decrease relative power in the frequency bin containing the dominant peak. A. and B. show representative inspiratory bursts and average power spectra, respectively, from a single P9 slice. C. and D. show representative inspiratory bursts and average power spectra, respectively, from a different P9 slice. In B, Substance P causes the relative power in the frequency bin containing the dominant peak (dotted lines) to increase. In D, average power spectra show that the relative power of the frequency bin containing the dominant peak (dotted lines) does not change with Substance P bath application. E. Although Substance P increases the relative power of oscillations, this effect is not statistically significant (72 ± 33%, n = 8, n.s.). Oscillation power was not different from control following wash (-45 ± 13%, n = 6, n.s.).

(Figure 2.8D). A summary of the effect of Substance P on relative power of the oscillations is shown in Figure 2.8E. When data from all 8 slices were pooled, bath application of Substance P does not significantly affect relative power (72 ± 33%, n = 8, n.s.). Following washout, oscillation power was not different from control (-45 ± 13%, n = 6, n.s.).

These data reconfirm that Substance P increases slice excitability by increasing peak integrated activity and inspiratory burst frequency. $GABA_A$ and GlyR blockade results in a similar increase in peak integrated activity. However, increasing slice excitability by Substance P bath application does not reduce oscillation power. In fact, bath application of Substance P increases oscillation power in the majority of slices tested. These data demonstrate that the reduction in oscillation power following $GABA_A$ and GlyR blockade is not a result of increased slice activity and provides further evidence that GABAergic and glycinergic transmission have a unique role in synchronizing inspiratory neurons on a short time-scale.

Prolonging GABAergic Current Decreases Oscillation Frequency

I have demonstrated that GABAergic transmission is important in modulating respiratory rhythm and in synchronizing inspiratory motoneurons, because blocking GABAergic current increased peak integrated activity and decreased oscillation power, respectively. Therefore, I next investigated the effect of prolonging the time course of GABAergic transmission on inspiratory motoneuron synchronization and inspiratory rhythm by bath applying zolpidem to the slice. Previous studies have shown that zolpidem prolongs the time course of GABAergic IPSCs recorded from cerebellar and hippocampal neurons (Vicini et al., 2001; Goldstein et al., 2002).

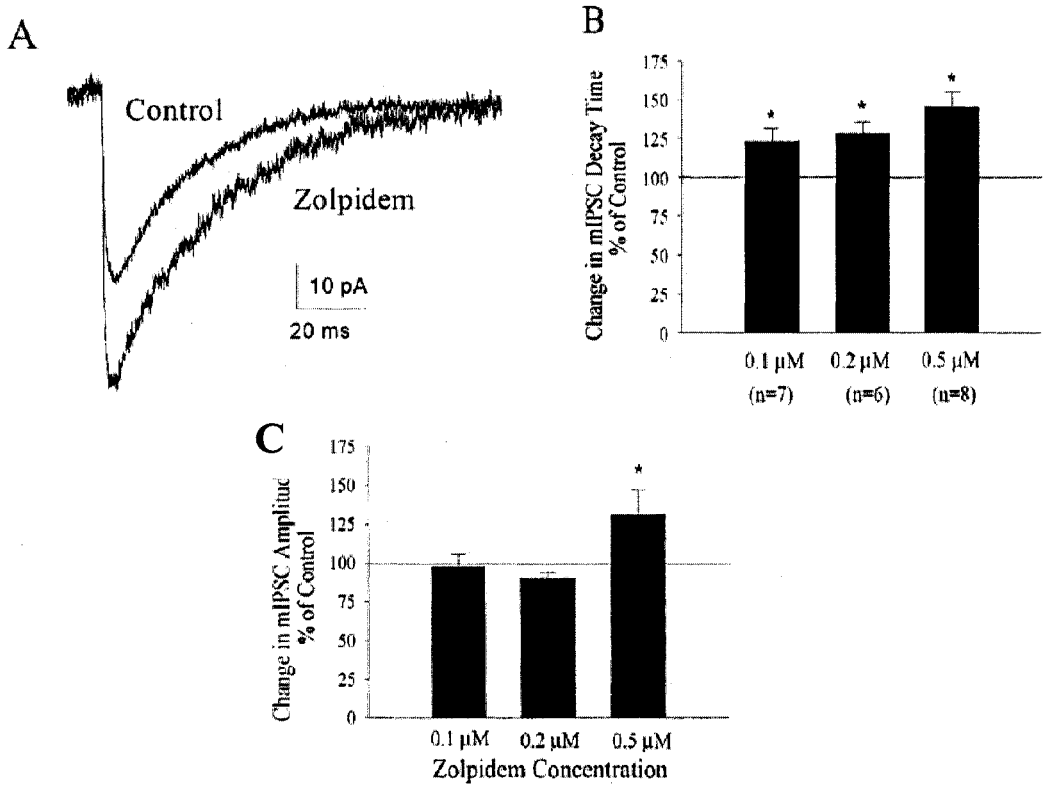

Figure 2.9. Effects of zolpidem on the amplitude and decay time of $GABA_A$ receptor-mediated mIPSCs recorded from hypoglossal motoneurons. A. Superimposed average GABAergic mIPSCs recorded in a cell (P8 mouse) in control and after 0.5 μM zolpidem. In this cell, the decay time increased fr0m 21.3 ms in control to 27.4 ms after zolpidem (Zolp), while amplitude increase from 46 pA in control to 70 pA after Zolp. B. Change in GABAergic mIPSC decay time as a percent of control in response to bath application of 0.1, 0.2, or 0.5 μM Zolp. Asterisk indicates significantly different change from control ($p < 0.05$). Zolp increased decay time at all concentrations tested. C. Change in GABAergic mIPSC amplitude as a percent of control. GABAergic mIPSC amplitude increased only at the highest concentration of Zolp tested. Data are expressed as means ± SE with the number of cells indicated in parentheses. Amplitude and decay times were calculated from a total of 1089 (0.1 μM Zolpidem), 555 (0.2 μM), and 703 (0.5 μM) miniature events.

We confirmed these results in our system by recording $GABA_A$ receptor-mediated mIPSCs from juvenile HMs (P8-10) in the non-rhythmically active brainstem slice preparation in control and following bath application of 0.1, 0.2, and 0.5 μM zolpidem. The representative average GABAergic mIPSCs in the left panel of Figure 2.9A are normalized to baseline and show the increase in mIPSC peak amplitude and decay time following bath application of 0.5 μM zolpidem. Bath application of 0.1, 0.2,

and 0.5 μM zolpidem increased GABAergic mIPSC decay time by 23 ± 8, 27 ± 8, and 45 ± 10%, respectively (Figure 2.9B). In addition to the increase in decay time, 0.5 μM zolpidem increased mean mIPSC peak amplitude by 31 ± 16 % (Figure 2.8C).

Next, I investigated the effects of prolonging GABAergic currents on inspiratory activity and oscillation frequency recorded from XII nerve rootlets in the rhythmic slice preparation. By pharmacologically prolonging the time course of inhibition with zolpidem, I expected to decrease oscillation frequency. Synchronous oscillations within an inspiratory burst are characterized by clusters of action potentials that are separated by gaps of little or no activity. I hypothesized that inhibitory synaptic transmission contributes to the gaps of no activity (Figure 1.1) and that by increasing the decay time of GABAergic currents, the duration of these gaps would also increase. This effect would be reflected in the XII nerve recording as a decrease in oscillation frequency.

To test this hypothesis, I first bath applied strychnine then strychnine and zolpidem (0.1-0.5 μM) to rhythmically active slice preparations from P9-10 mice. Bath application of strychnine alone did not affect median oscillation frequency (-5 ± 2 %, n=7, n.s., paired t-test). An example of the unchanging oscillation frequency, following strychnine bath application, is shown in the average power spectra of Figure 2.3B. For 7 rhythmic slices where it was tested, subsequent bath application of strychnine and zolpidem reduced average median oscillation frequency from 35 ± 3 Hz, in the presence of strychnine, to 33 ± 3 Hz following combined strychnine and zolpidem bath application (-9 ± 2 %, n=7, $p < 0.01$, paired t-test). The average power spectra in Figure 2.10A and B show the decrease in median oscillation frequency following strychnine and zolpidem (Stry + Zolp) bath application relative to strychnine application alone.

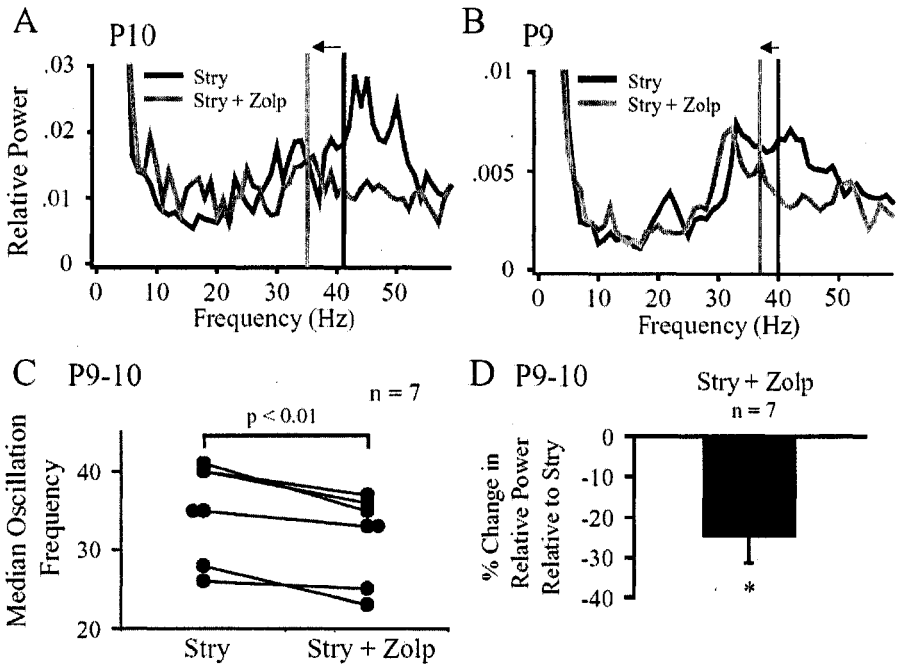

Figure 2.10. Zolpidem (Zolp) bath application decreased median oscillation frequency. A. Average power spectra in Stry and following bath application of Stry + 0.1 μM Zolp in a P10 mouse slice. Median oscillation frequency decreased from 41 Hz in Stry to 35 Hz following bath application of Stry + Zolp. In A and B, median oscillation frequencies in the presence of Stry and Stry + Zolp are represented by the black and gray lines, respectively. Leftward arrows (A and B) indicate direction of frequency shift. B. Average power spectra in Stry and following bath application of Stry + 0.2 μM Zolp in a P9 mouse slice. Median oscillation frequency decreased from 40 Hz in Stry to 37 Hz following bath application of Stry + Zolp. C. Median oscillation frequency decreased in the presence of Stry + Zolp (0.1-0.5 μM) relative to Stry alone D. Summary data showing the decrease in relative power of oscillations following bath application of Stry + Zolp (0.1-0.5 μM) relative to Stry alone. Mean ± SE. (*, $p < 0.05$)

For this sample of 7 rhythmic slices, I observed that bath application of strychnine alone did not decrease the relative power of oscillations (-19 ± 11%, n = 7, p = 0.06). Relative to strychnine, which acts as the control condition in this set of experiments, combined bath application of strychnine and zolpidem reduced oscillation power (Figure 2.10D: -25 ± 7%, n = 7, $p < 0.05$). Relative to the effect of strychnine alone, combined bath application of strychnine and zolpidem decreased peak integrated activity (-24 ± 12 %, n = 7, $p < 0.05$) and burst duration (-12 ± 2 %, n = 7, $p < 0.01$).

Discussion

In the present work, I have investigated inspiratory-phase short time-scale synchronization of HMs during postnatal development and the role of GABAergic and glycinergic transmission in generating inspiratory-phase oscillations. My principal findings are threefold. First, the frequency of synchronous oscillations increases with postnatal development in P0-11 mice. Second, both GABAergic and glycinergic transmission are required to generate robust oscillations in P0-10 mice. Third, prolonging the decay time of GABAergic currents with zolpidem reduces median oscillation frequency.

Changes in GABAergic and Glycinergic Transmission During Postnatal Development

In the rodent brainstem, GABAergic and glycinergic transmission undergo many changes during the first two weeks of postnatal development, two of which are most relevant to this study. One of these changes is the decrease in the GABAergic and glycinergic current decay times (Singer et al., 1998; Sebe et al., 2003) that occur in parallel to shifts in the $GABA_A$ and GlyR subunit compositions, respectively (Singer et al., 1998; Liu and Wong-Riley 2004; Liu and Wong-Riley 2005). As the postnatal rodent develops, the decay time of GABAergic and glycinergic mIPSCs recorded from HMs decreases (Singer et al., 1998; Sebe et al., 2003). The shortening of inhibitory currents may be partially responsible for the increase in oscillation frequency I observed with postnatal development. Synchronized oscillations during an inspiratory burst are characterized by clusters of action potentials separated by periods of little or no activity. The time course of inhibitory currents may determine for how many milliseconds the

inspiratory motoneurons are inactive (Palva et al., 2000), during an inspiratory burst, until the next cluster of action potentials occurs.

In addition to the change in mIPSC kinetics, inspiratory neurons undergo a shift in the Cl^- reversal potential during postnatal development. (Singer et al., 1998; Ritter and Zhang 2000). The Cl^- reversal potential shifts from a depolarizing to a hyperpolarizing potential as more of the KCC2 transporter, which extrudes Cl^- from the cell, is expressed (Rivera et al., 1999). Given that the Cl^- reversal potential is still depolarized during postnatal development in brain regions such as the hippocampus (Cherubini et al., 1991), it is at first puzzling that GABAergic and glycinergic transmission are inhibitory in the newborn respiratory network. However, many studies, including the present work, have repeatedly shown that blocking $GABA_A$ and GlyRs in the neonatal mouse respiratory network elevates inspiratory activity (Paton and Richter 1995b; Ramirez et al., 1996; Bou-Flores and Berger 2001). These results demonstrate that Cl^- mediated transmission suppresses excitability in the respiratory network even in newborn mice.

Mechanistically, the inhibitory effect of GABAergic and glycinergic transmission in the newborn respiratory network may be explained by a combination of a perinatally occurring shift in the Cl^- reversal potential in PBC neurons and shunting inhibition in inspiratory motoneurons. In PBC inspiratory neurons, the shift in the Cl^- reversal potential is complete by embryonic day 19 (Ren and Greer 2006). Soon after birth, rat HMs reach their hyperpolarized Cl^- reversal potential between postnatal day 3 and 10 (Singer et al., 1998). Despite the depolarized Cl^- reversal potential in neonatal inspiratory motoneurons, the activation of $GABA_A$ and GlyRs can produce shunting inhibition by decreasing the cell input resistance. Shunting inhibition has been

demonstrated to suppress firing in P0-4 HMs (Marchetti et al., 2002). Therefore, GABA and glycine mediate inhibitory transmission in the postnatal respiratory network.

Prolonging the Decay Time of GABAergic Currents Decreases Median Oscillation Frequency

By employing a network model, Pauluis et al. demonstrated that prolonging the time course of inhibitory currents decreased oscillation frequency (Pauluis et al., 1999). In a study of cholinergically induced hippocampal oscillations, Fisahn et al. demonstrated that prolonging the time course of GABAergic transmission by bath application of pentobarbital decreased the oscillation frequency (Fisahn et al., 1998). In the present experiment, I pharmacologically prolonged the decay time of GABAergic currents in the inspiratory network with zolpidem and found that median oscillation frequency decreased. Further evidence for zolpidem's action on the inspiratory network are the decrease in peak integrated activity and burst duration following bath application of zolpidem. Together, these findings support the hypothesis that time course of inhibitory currents are a determinant of oscillation frequency.

Blocking GABA and Glycinergic Transmission Disrupts Inspiratory Burst Frequency

When all inspiratory bursts were counted, I found that $GABA_AR$ blockade alone did not significantly affect inspiratory burst frequency in neonates or juveniles. This result is inconsistent with previous *in vitro* studies, using rodents and turtles, in which blocking $GABA_ARs$ was sufficient to increase inspiratory burst frequency (Hayashi and Lipski 1992; Ritter and Zhang 2000; Bou-Flores and Berger 2001; Johnson et al., 2002). I suspect that the reason for this discrepancy is the nonsaturating concentration

of the $GABA_AR$ antagonist, SR95531 (0.5 μM) I used. When we recorded GABAergic mIPSCs from HMs in the nonrhythmically active brainstem slices, 0.5 μM SR95531 blocked most but not all GABAergic mIPSCs (data not shown). However, I selected this nonsaturating concentration of SR95531 based on data from preliminary experiments in which I recorded inspiratory phase activity from the rhythmically active brainstem slice. In these experiments, I found that bath application of strychnine (1 μM) and a saturating concentration of SR95531 (1 μM), together, induced continuous seizure-like activity (data not shown). I was unable to perform power spectral analysis on this continuous seizure-like activity because I could not distinguish individual inspiratory bursts. To circumvent this problem, I used a nonsaturating concentration of SR95531 that increased peak integrated activity, when applied alone, without inducing continuous seizure-like activity, when applied with a saturating concentration of strychnine. This approach was used to fulfill the primary purpose of the present work that is to examine the role of GABA and glycine in generating inspiratory motoneuron synchronization.

As seen with the nonsaturating concentration of the $GABA_AR$ antagonist, GlyR blockade increased peak integrated activity without affecting inspiratory burst frequency. In the developmental time period I examined (P0-10), glycinergic transmission is still immature in the mouse brainstem (Singer et al., 1998; Kandler and Gillespie 2005). Therefore, measures of respiratory activity, such as inspiratory burst frequency, may be less sensitive to glycinergic modulation in an immature animal than in an adult. Consistent with this conclusion, *in vitro* and *in vivo* studies have shown that strychnine does not affect inspiratory burst frequency recorded from mice ranging from P0-14 (Paton and Richter 1995b; Lieske et al., 2000). However, the effects of GlyR blockade are still variable in this age range as strychnine increased inspiratory burst

frequency recorded from XII and C4 nerves from P0-5 mouse slices (Bou-Flores and Berger 2001). In mice P15 or older, a developmental stage at which the respiratory network is considered mature, GlyR blockade decreases inspiratory cycle length (Paton and Richter 1995b). Since that study by Paton et al., Pierrefiche et al. have demonstrated that strychnine increases in inspiratory burst frequency in adult animals (Pierrefiche et al., 1998). Although blocking $GABA_A$Rs or GlyRs, separately, did not increase inspiratory burst frequency blocking both forms of inhibition significantly elevated peak integrated activity.

In neonatal slices, when all inspiratory bursts were counted I found that $GABA_A$ and GlyR blockade induced a secondary rhythm, characterized by low amplitude and high frequency inspiratory bursts. Using the rhythmically active medullary slice preparation, Ritter and Zhang (Ritter and Zhang 2000) also recorded inspiratory activity from XII rootlets and reported a secondary rhythm following $GABA_A$ blockade with bicuculline. Using the mouse rhythmically active medullary slice preparation, Ramirez et al. recorded simultaneously from PBC neurons and a XII rootlet (Ramirez et al., 1996). They showed that PBC neurons fired inspiratory bursts at a higher frequency than XII rootlets. The secondary rhythm I observed may be generated by the PBC and not normally transmitted to the XII nucleus. When inhibitory synaptic transmission is blocked, the secondary rhythm generated in the PBC is revealed in XII motor output.

MFOs versus HFOs

As stated earlier, oscillations in the respiratory network are classified into MFOs and HFOs based on the frequency range in which they occur and the presence or absence, respectively, of oscillation coherence across different motoneuron

populations. Frequency range of the oscillations changes with many factors, including temperature (Richardson and Mitchell 1982), developmental age (Kocsis et al., 1999), and animal preparation used (Cohen et al., 1987; Liu et al., 1990; O'Neal, III et al., 2005). Although synchronous oscillations observed in the present work fall within the MFO range, oscillation frequency per se is not a reliable criterion in determining the MFO or HFO nature of synchronous oscillations because of the factors previously mentioned.

Without coherence analysis of synchronous oscillations, it is unknown whether the oscillations reported here are MFOs, which are generated at the motoneuron level, or HFOs, which are generated by a common medullary input. The present and prior work from this laboratory (Bou-Flores and Berger 2001), has shown that synaptic inhibition is required for the generation of robust inspiratory-phase oscillations. It is possible that the oscillations are MFOs that are generated within the XII motor nucleus itself, since this nucleus contains both motoneurons and a small population of inhibitory interneurons (Peever et al., 2002). During inspiration, HMs receive concurrent excitatory and inhibitory inputs (Saywell and Feldman 2004) that could be involved in producing such oscillations. Alternatively, the oscillations may be HFOs that are generated upstream of the motor nucleus, either within or outside of the PBC. Immunohistochemical studies have shown that the medullary reticular formation, in which a premotor area might be found, contains GABAergic and glycinergic neurons that project bilaterally to XII nuclei (Li et al., 1997; Travers et al., 2005). The PBC contains expiratory neurons that are sensitive to $GABA_A$ and GlyR antagonists (Shao and Feldman 1997) as well as GABAergic and glycinergic neurons (Liu and Wong-Riley 2004) which modulate the inspiratory rhythm (Pierrefiche et al., 1998).

In the next chapter, I investigate where in the rhythmically active medullary slice preparation synchronous oscillations are generated using a combination of approaches, including coherence analysis of left and right XII rootlet activity. By elucidating the origin of the oscillations, be they MFOs or HFOs, I can determine whether the oscillations recorded *in vitro* reflect localized synchrony in the motor nucleus (MFOs) or widespread synchronous activity across motor pools that is coordinated by a common medullary input (HFOs). In this regard, oscillations may be a window through which I can determine the degree of synchronous activity within the respiratory network.

Chapter 3: Possible Premotor Origin of Synchronous Oscillations in the Rhythmic Slice

Introduction

The origin of inspiratory-phase synchronous oscillations has been the subject of great interest since Cohen initiated an extensive study of these oscillations in 1973 (Cohen 1973). From the onset (Cohen 1973), oscillations have been classified into two categories that are termed high and medium frequency oscillations (HFOs and MFOs). Cohen and colleagues (Cohen et al., 1997) hypothesized that the characteristics that distinguish HFOs from MFOs actually reflect where in the respiratory network synchronous oscillations are generated.

The defining characteristic of HFOs is that they are coherent across different respiratory motor pools (phrenic, laryngeal and hypoglossal nerves) (Cohen et al., 1987) and bilaterally coherent within the same motor pool (left vs. right phrenic nerves)(Christakos et al., 1991). Thus, HFOs recorded from different nerves occur at the same frequency. Further, crosscorrelation analysis of HFOs recorded from the left and right phrenic nerves (Christakos et al., 1991) have demonstrated that oscillations not only share spectral properties but that the action potentials in the left and right phrenic nerves are temporally correlated on a short time scale. The temporal correlation of HFOs recorded from different motor pools strongly suggests that they are generated by a common input somewhere upstream of the motoneurons (Kirkwood et al., 1982; Cohen et al., 1987). It is thought that the inspiratory pattern generator is a likely source of this shared input because its propagates inspiratory rhythm to numerous respiratory motor pools (Cohen et al., 1997).

Like HFOs, MFOs are widespread in that they have been recorded from multiple respiratory motoneurons and nerves (Cohen et al., 1997; Funk and Parkis 2002). However, the MFO coherence between different respiratory nerves and across bilateral nerves derived from the same motor pool is rare or weak (Cohen et al., 1987; Christakos et al., 1991). Therefore, although MFOs are present in different nerves, they do not occur at the same frequency. In contrast to HFOs, it is likely that MFOs are individually generated in (Cohen et al., 1997) or immediately upstream of each motor pool by premotor neurons (Kirkwood et al., 1982). This would explain the lack of MFO coherence across different motoneurons and nerves.

Coherence and cross-correlation analyses have directed us toward the possible regions of the respiratory network in which HFOs and MFOs are generated, but these regions have not yet been tested. The simplified network within the rhythmically active medullary slice preparation affords such a test of the candidate regions. Within the rhythmic slice, the inspiratory pattern generator and the inspiratory motor pool, which correspond to the proposed origins of HFOs and MFOs, are the PBC and the XII nucleus, respectively. The premotor area, which lies between the PBC and the XII nucleus, may also be involved in generating MFOs, but the location of this region in the rhythmic slice preparation is yet to be identified.

In this chapter, I tested whether inspiratory-phase synchronous oscillations exhibited by XII rootlets in the rhythmic slice preparation are generated in the PBC or in, or immediately upstream of, the XII nucleus. To do this, I locally and unilaterally perfused ACSF containing high K^+ to the PBC or the XII nucleus. High

K^+ increases neuronal excitability by raising the resting membrane potential near threshold and increasing the probability that a neuron will fire.

Given that the PBC is the locus of inspiratory rhythm generation and that the left and right PBCs are bilaterally connected, increasing the excitability of the PBC unilaterally should increase the inspiratory burst frequency bilaterally. If inspiratory-phase synchronous oscillations in the slice preparation are generated at the PBC level, that is if they are HFOs, the same manipulation should also increase the power of oscillations bilaterally.

Locally increasing neuronal excitability in the unilateral XII nucleus, in contrast, should have no effect on the inspiratory burst frequency because inspiratory motoneurons are not involved in rhythm generation. Instead, High K^+ application to the XII nucleus should increase the peak integrated activity of inspiratory bursts recorded from XII rootlets. This hypothesis is supported by previous studies in which local and unilateral perfusion of non-NMDA receptor (non-NMDAR) antagonists to the XII nucleus had no effect on inspiratory burst frequency but increased the peak amplitude of inspiratory bursts recorded from the XII rootlets (Funk et al., 1993). With respect to the effect on short time scale synchrony, unilateral high K+ application to the XII nucleus should increase oscillation power unilaterally if synchronous oscillations are MFOs that are generated at or immediately upstream of the HM level.

I also applied crosscorrelation and coherence analysis of inspiratory-phase motor discharge recorded bilaterally from XII rootlets to determine the origin of oscillations. If bilaterally recorded oscillations are temporally correlated and strongly coherent, they are probably generated in the PBC. If the oscillations are

not temporally correlated and are weakly coherent at best, they are likely generated in or immediately upstream of the XII nucleus

Methods

Slice Preparation

In vitro experiments were performed on the rhythmically active medullary slice preparation (Figure 3.1A and 3.2A) from Swiss-Webster mice (P4-7). Mice were anesthetized with isoflurane and sacrificed by decapitation in accordance with the regulations of the University of Washington Institutional Animal Care and Use Committee (IACUC).

Methods used in dissecting the rhythmically active medullary slice preparation have been described previously (Funk et al., 1993; Sebe et al., 2006). In brief, the medulla and cervical spinal cord were isolated and removed from the mouse. The brainstem and spinal cord were pinned onto a Sylgard® block and the block was mounted into a vibratome platform (Pelco 101 Series 1000, Redding, CA). Brainstem slices were then cut from rostral to caudal. After the facial nucleus was no longer visible, another 200 μm slice was cut prior to cutting the rhythmic slice. The thickness of the rhythmic slice was increased from 500-700 μm depending on the age of mouse. Slices from younger mice were thinner than those obtained from older mice. This slice was placed into the recording chamber and superfused for at least 20 minutes with 8 mM K^+ ACSF before recording began.

Recording

For the rhythmically active slice preparation, the temperature of the custom-made recording chamber was maintained between 27 and 28°C. Glass suction electrodes were pulled from borosilicate glass and filled with ACSF to record from the cut ends of XII rootlets. Raw nerve signals were sampled at 5 kHz, amplified, AC filtered at 0.1 Hz and low pass filtered at 2 kHz using CyberAmp 320 and pClamp8 (Axon Instruments, Union City, CA). To measure integrated nerve activity, the filtered signal was rectified and integrated using a custom built "leaky" integrator with a time constant of 100 ms.

Solutions

The normal ACSF used for rhythmically active slice preparations contained (in mM): 118 NaCl, 3 KCl, 1 $MgCl_2$, 1 NaH_2PO_4, 25 $NaHCO_3$, 30 D-glucose and 1.5 $CaCl_2$. The osmolarity of the ACSF was 300 mOsm and the ACSF was pH adjusted to 7.4 with NaOH. For recording spontaneous rhythmic activity, the same ACSF was used except that KCl concentration was elevated to 8 mM KCl. ACSF was superfused over the preparation at 2-3 ml/min and recycled using a peristaltic pump (Rainin). For local perfusion, ACSF contained fast green (11.2mg/100ml) or varying concentrations of K^+ (8, 20, 60 or 80 mM).

Local Perfusion

In each experiment, ACSF containing the control concentration of K^+ (8mM) and, subsequently, a higher concentration of K^+ were locally perfused to the PBC or XII nucleus unilaterally. In numerous preliminary experiments, the PBC was located using a

combination of ventrolateral landmarks (i.e. inferior olive and nucleus ambiguus) and field electrode recordings of inspiratory activity in the PBC. Knowledge acquired from these preliminary experiments regarding the location of the PBC with respect to ventrolateral landmarks was used to target the PBC for local perfusion. For unilateral excitation of the XII nucleus, the XII nucleus and its borders were easily identified visually. The local perfusate was delivered in the direction parallel to the flow path of the bath perfusate. To do this, a local perfusion pipette was placed just above the surface of the slice and at the upstream border of the target region (unilateral PBC or XII nucleus). The local perfusate was rapidly removed using a local uptake pipette placed downstream of and within 0.5 mm of the local perfusion pipette. The local uptake pipette was positioned so that the local perfusate was limited to the target region. To visualize the spread of the local perfusate, fast green was included in all locally perfused ACSF solutions. Control experiments demonstrated that local perfusion of fast green alone had no effect on inspiratory-phase activity and synchronous oscillations (data not shown, n=3). I documented the region onto which the perfusate was applied by capturing a digital image of the spread of fast green during the experiment (Figure 3.1A and 3.2A). Due to the anatomy of the rhythmic slice, the slice needs to be positioned rostral (Figure 3.1A) or caudal (Figure 3.2A) side up to expose the PBC or XII nucleus, respectively. In order to locally perfuse the PBC and, sequentially, the XII nucleus using the same rhythmic slice, the XII rootlets would need to be expelled from suction electrodes and the slice flipped. Therefore, for each rhythmic slice the local perfusate was unilaterally applied only to the PBC or the XII nucleus.

For experiments in which ACSF was locally perfused onto the PBC, ACSF containing 8 mM and, subsequently, 60 or 80 mM K^+ were locally applied. For experiments in which ACSF was locally perfused onto the XII nucleus, ACSF containing 8 mM and, subsequently, 20 mM K^+ were applied. The K^+ concentrations in the local perfusates were experimentally determined. For unilateral perfusion of the PBC, 60 mM K^+ was the lowest concentration tested (30, 40, 60 and 80 mM) that had an effect on inspiratory activity. With respect to the XII nucleus, 20 mM K^+ was the lowest concentration tested (30, 40, 60 and 80 mM) that induced an effect on inspiratory activity. K^+ concentrations greater than 30 mM (40, 60 and 80 mM) induced high levels of tonic activity in the XII rootlet recording that masked the inspiratory bursts. However, when inspiratory bursts could be distinguished from the tonic activity, there was no change in inspiratory burst frequency following local and unilateral perfusion of high K^+ onto the XII nucleus (data not shown). I switched between perfusate solutions using an in house valve box that controlled the solution that passed through a miniature manifold connected to the local perfusion pipette. The time at which the solution was switched was digitally recorded using an output from the valve box to the AD converter. To minimize dead space in the perfusion pipette, perfusate was delivered from the manifold to the tip of the pipette via quartz capillary tubing. For all experiments, switching to a perfusate containing elevated K^+ rapidly (within 3 minutes following the switch) elicited an increase in XII rootlet activity (PBC: increase in inspiratory burst frequency, XII nucleus: increase in peak integrated activity).

Data Analysis

Inspiratory bursts were selected in Clampfit (Axon Instruments) and analyzed in Igor Pro (Wavemetrics, Inc) using routines developed by Dr. Randy K. Powers. For each recording condition, 6-20 inspiratory bursts were selected and used to create 6-20 absolute power spectra in which the frequency resolution was 1-2 Hz. Average absolute power spectra were computed by averaging the 7-20 absolute power spectra for each condition. Average relative power spectra were calculated from the average absolute power spectra by dividing the absolute power at each data point (0-99 Hz) by the absolute power for all data points (0-99 Hz). Average relative and absolute power spectra were used to compute changes in the relative power of oscillations and in the coherence between left and right XII rootlet activity, respectively.

To measure the relative power of synchronous oscillations, I located the dominant peaks in the average relative power spectra that I computed from inspiratory bursts recorded in the control condition and following local perfusion of high K^+. For each pair of average relative power spectra, I used the dominant peak with the greater relative power value to define the location of a 10 Hz bin. The 10 Hz bin was centered on the frequency at which the dominant peak occurred. I computed the fraction of relative power within the 10 Hz bin. To do this, I added all points within the 10 Hz bin containing the dominant peak and divided that number by the total relative power from 0-99 Hz. By computing the fraction of relative power for each recording condition, I measured changes in the relative power of synchronous oscillations following local perfusion of high K^+. Paired t-tests were used to compare changes in relative power between control and elevated K^+ conditions.

Cross-correlation histograms (CCHs) of left and right XII rootlet activity were computed (Igor Pro) using the same 6-20 inspiratory bursts selected for power spectra and coherence analysis. For each pair of inspiratory bursts, the spike times in the left and right rootlet recordings were amplitude discriminated as previously done for multiunit recordings acquired using the rhythmic slice preparation (Peever and Duffin 2001; Li et al., 2003). Next, the time lags between the occurrence of a given spike in the left rootlet recording and the occurrences of all spikes in the right XII rootlet recording were measured. The CCHs computed for each inspiratory burst were averaged and the y-axis of the average CCH was normalized relative to the total number of spikes in the left rootlet recording. Therefore, the y-axis reflects the probability of occurrence of a spike in each bin along the x-axis. In computing all CCHs, inspiratory motor discharge recorded from the XII rootlet ipsilateral and contralateral to local perfusion were used as the "stimulus" and "response", respectively. The bin width for all CCHs was set at 1 ms. For each CCH, the strength of synchronization was expressed as the *k* ratio as previous done for CCHs of single and multiunit recordings acquired from respiratory neurons (Sears and Stagg 1976; Graham and Duffin 1981; Li et al., 2003). The *k* ratio is defined as the ratio of the total counts in the peak region of the CCH to the mean bin count in the region of the CCH outside of the peak (Nordstrom et al., 1992). To determine the statistical significance of the peak, I estimated the variance of the *k* ratio (σ_k^2) as: $\sigma_k^2 = k^*(\sigma_{baseline}^2 / m_{baseline}^2)$, where *k* is the *k* ratio and $\sigma_{baseline}^2$ and $m_{baseline}$ are the variance of the bin count and the mean bin count, respectively, of the region outside the peak. The peak was statistically significant at $p<0.05$ if $k > 1.96$ * the square root of σ_k^2 (Sears and Stagg 1976; Moore and McCabe 1999). The half amplitude width was computed by determining the time at

which the peak in the CCH was at half amplitude. All values are expressed as mean ± s.e.. Paired t-tests were used to compare changes in half amplitude width, time lag of peak, and total counts in the peak region between control and elevated K^+ conditions.

Coherence plots of left and right XII rootlet activity were computed to determine whether the frequency of synchronous oscillations was the same bilaterally. Each coherence plot was computed from the average absolute power spectra for the left and right rootlet recordings and the cross spectra of the two average absolute power spectra. For each coherence plot, data points were in 1-2 Hz intervals. By incorporating the number of inspiratory bursts used to make each coherence plot, upper 95% confidence limits were calculated using the following equation: upper 95% confidence limit = $1-(0.05)^{1/(n-1)}$ where n = # of inspiratory bursts selected for analysis. The upper 95% confidence limit is shown as a horizontal dashed line on the coherence plot in Figure 3.7C. Coherence values above this line are significantly different from zero and are evidence for the presence of correlation between the left and right XII rootlet activity at a given frequency (Halliday and Rosenberg 2006). For each coherence plot, the value of significant coherence was computed from 0-100 Hz. Paired t-tests were used to compare changes in the coherence greater than the confidence limit between control and elevated K^+ conditions.

Peak integrated activity and burst duration were measured in Igor Pro using the rectified and integrated traces of the inspiratory bursts. Peak integrated activity was the highest point of the rectified and integrated traces. Burst duration was defined as the time at 95% of the integrated area subtracted by time at 5% of the integrated area. Peak integrated activity and burst duration values were computed for the same 6-20 inspiratory bursts used for power spectral analysis. The average peak integrated

activity and burst duration were compared across recording conditions. Paired t-tests were used to determine statistical significance of changes in peak integrated activity, inspiratory burst duration and inspiratory burst frequency, separately, between control and elevated K^+ conditions. Following unilateral excitation of the XII nucleus, I observed an increase in peak integrated activity recorded from the ipsilateral and contralateral XII rootlet recordings. To determine whether this change in peak integrated activity was statistically different between the two sides, I applied a single factor analysis of variance (ANOVA).

Results

Unilateral Excitation of the PBC, but Not the XII nucleus, Increases Mean Inspiratory Burst Frequency Recorded Bilaterally

In each experiment, I used the rhythmically active medullary slice preparation to record inspiratory-phase activity from the left and right XII rootlets while bathing the slice in ACSF containing 8mM K^+. In this recording condition, I locally and unilaterally perfused the PBC (Figure 3.1A) or the XII nucleus (Figure 3.2A) with control ACSF (8mM K^+) containing fast green. Next, I switched the local perfusate to ACSF containing a higher concentration of K^+ and the same concentration of fast green. Fast green was included in all local perfusate solutions to monitor the spread of ACSF containing the dye and to ensure that the dye remained localized to the unilateral PBC or XII nucleus. For local perfusion of high K^+ onto the unilateral PBC, 60 or 80 mM K^+ was necessary to elicit an increase in inspiratory activity. For local perfusion of high K^+ onto the unilateral XII, 20 mM high K^+ was sufficient to increase inspiratory activity.

First, I examined the effect of unilateral excitation of the PBC on parameters of long time scale synchrony, that is on mean inspiratory burst frequency, mean peak integrated activity and mean burst duration. Although two concentrations of K^+ were locally perfused into the unilateral PBC, the effects of 60 and 80 mM K^+ on inspiratory activity were not differentiable. Therefore, data from experiments using the two K^+ concentrations were pooled. Unilateral excitation of the PBC increased mean inspiratory burst frequency bilaterally by 226 ± 49% (ipsilateral and contralateral: control: 0.09 ± 0.006 Hz, high K^+: 0.31 ± 0.06 Hz, n=10, $p< 0.01$) (Figure 3.1B and C). For all experiments in which inspiratory activity was recorded bilaterally, each inspiratory burst in the left rootlet recording was matched by a simultaneously occurring inspiratory burst in the right rootlet recording. Local perfusion of high K^+ had no effect on mean peak integrated activity of inspiratory bursts recorded from the ipsilateral (IPSI: increased by 10 ± 5 %, n=10, n.s.) and contralateral (CONTRA: increased by 7 ± 4 % of control, n = 10, n.s.) XII rootlets (Figure 3.1D). Unilateral excitation of the PBC also had no effect on mean inspiratory burst duration recorded from the ipsilateral (increased by 1.7 ± 1.3%; control: 698 ± 187 ms, high K^+: 792 ± 194 ms, n=10, n.s.) and contralateral (increased by 0.3 ± 1.3%; control: 821 ± 319 ms, high K^+: 796 ± 288 ms; n=10, n.s.) XII rootlets (Figure 3.1E).

Next, I investigated the effect of unilateral excitation of the XII nucleus on the long time scale parameters. In contrast to the effect of unilateral excitation of the PBC, unilateral excitation of the XII nucleus, did not affect mean inspiratory burst frequency bilaterally (IPSI and CONTRA: increased by 15 ± 7 %; control: 0.09 ± 0.01 Hz, high K^+: 0.10 ± 0.01 Hz, n=10, n.s.)(Figure 3.2C). However, local unilateral perfusion of high K^+ to the XII nucleus increased mean peak integrated activity by 33 ± 5 % (n=10, $p<0.001$)

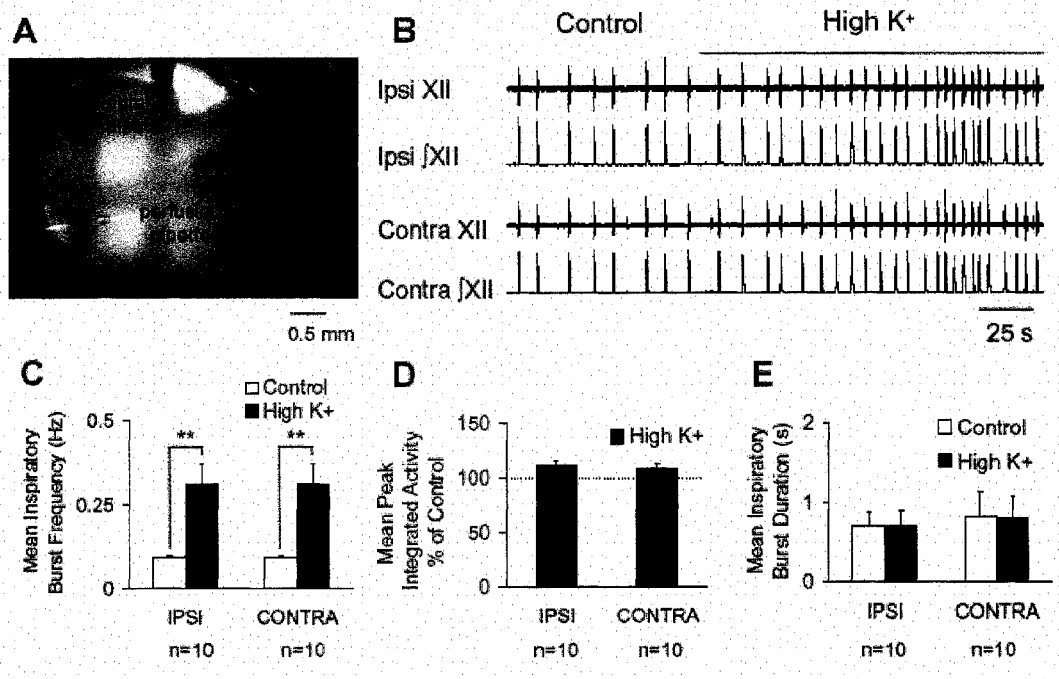

Figure 3.1: Local unilateral perfusion of high K^+ to the PBC bilaterally increases inspiratory burst frequency. A. Local perfusion of ACSF containing fast green to the unilateral PBC of a rhythmically active medullary slice preparation. Perfusion region is circumscribed to a zone less than 0.5 mm in diameter as revealed by fast green labeled region over the left PBC. Asterisk is over epoxy bead on a nylon thread that helps to limit the labeled perfusion region. Arrows indicate the local perfusion pipette and the local uptake pipette. B. Representive raw (XII) and rectified and integrated (∫XII) hypoglossal rootlet recordings from the ipsilateral (Ipsi) and contralateral (Contra) hypoglossal rootlets. Local perfusion of high K^+ (80 mM) to the unilateral PBC bilaterally increases inspiratory burst frequency (B and C) by 226 ± 49% (n=10, $p<0.01$). D and E. Unilateral excitation of PBC has no effect on peak integrated activity (IPSI: increased by 10 ± 5%;CONTRA: increased by 7 ± 4%; n=10, n.s.) or on inspiratory burst duration bilaterally (IPSI: increased by 1.7 ± 1.3%;CONTRA: increased by 0.3 ± 1.3%; n=10, n.s.)

in the ipsilateral rootlet recording (Figure 3.2B and D) and in the contralateral rootlet recording (by 14 ± 4 %; n=10, $p<0.05$) (Figure 3.2 B and D). Although the percent increase in peak integrated activity observed in the ipsilateral rootlet recording was greater than that measured in the contralateral rootlet recording, the effects were not statistically different (single factor ANOVA, $p>0.05$). As in Figure 3.1E, unilateral excitation of the XII nucleus had no effect on mean inspiratory burst duration in the ipsilateral (increased by 1 ± 4 %; control: 537 ± 24 ms, high K^+: 538 ± 14 ms, n=10,

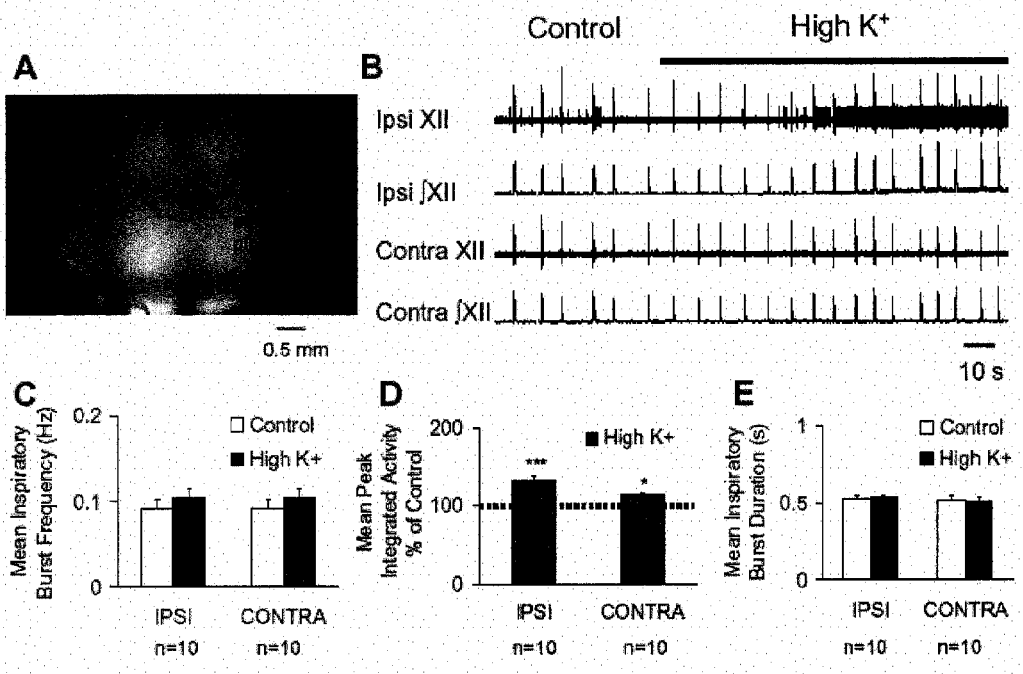

Figure 3.2: Local unilateral perfusion of high K^+ to the XII nucleus bilaterally increases inspiratory burst frequency. A. Local perfusion of ACSF containing fast green to the unilateral XII nucleus of a rhythmically active medullary slice preparation. Perfusion region is circumscribed to a zone less than 0.5 mm in diameter as revealed by fast green labeled region over the left XII nucleus. Asterisks are over epoxy beads on a nylon thread that help to limit the labeled perfusion region. Arrows indicate the local perfusion pipette and the local uptake pipette. B. Representive raw (XII) and rectified and integrated (∫XII) hypoglossal rootlet recordings from the Ipsi and Contra hypoglossal rootlets. B and C. Local perfusion of high K^+ to the unilateral XII nucleus has no effect on inspiratory burst frequency measured bilaterally (IPSI and CONTRA: increased by 15 ± 7%; n=10, n.s.). D. Unilateral excitation of the XII nucleus increased peak integrated activity in the IPSI rootlet (33 ± 5%, n=10, $p<0.001$) and in the CONTRA rootlet (14 ± 4%, n=10, $p<0.05$). E. There was no effect on mean inspiratory burst duration measured bilaterally (IPSI: increased by 1.1 ± 2.8%; CONTRA: increased by 0.3 ± 2.1%; n=10, n.s.)

n.s.) or the contralateral rootlet recording (decreased by 0.3 ± 2 %; control: 529 ± 27 ms, high K^+: 524 ± 20 ms; n=10, n.s.) (Figure 3.2E).

Unilateral Excitation of the XII Nucleus, but Not the PBC, Increases Oscillation Power

I investigated the effect of unilateral excitation of the PBC or XII nucleus on the relative power of oscillations recorded from the ipsilateral and contralateral XII rootlets. To do this, I computed average relative power spectra for inspiratory bursts recorded from the ipsilateral and contralateral XII rootlets in control conditions and following local

unilateral perfusion of high K^+ to the PBC or XII nucleus. Representative raw filtered (1-200 Hz bandpass) inspiratory bursts recorded from the ipsilateral and contralateral XII rootlets in the control condition and following unilateral local perfusion of high K^+ onto the PBC are shown in Figures 3.3A and B. The top traces are inspiratory bursts

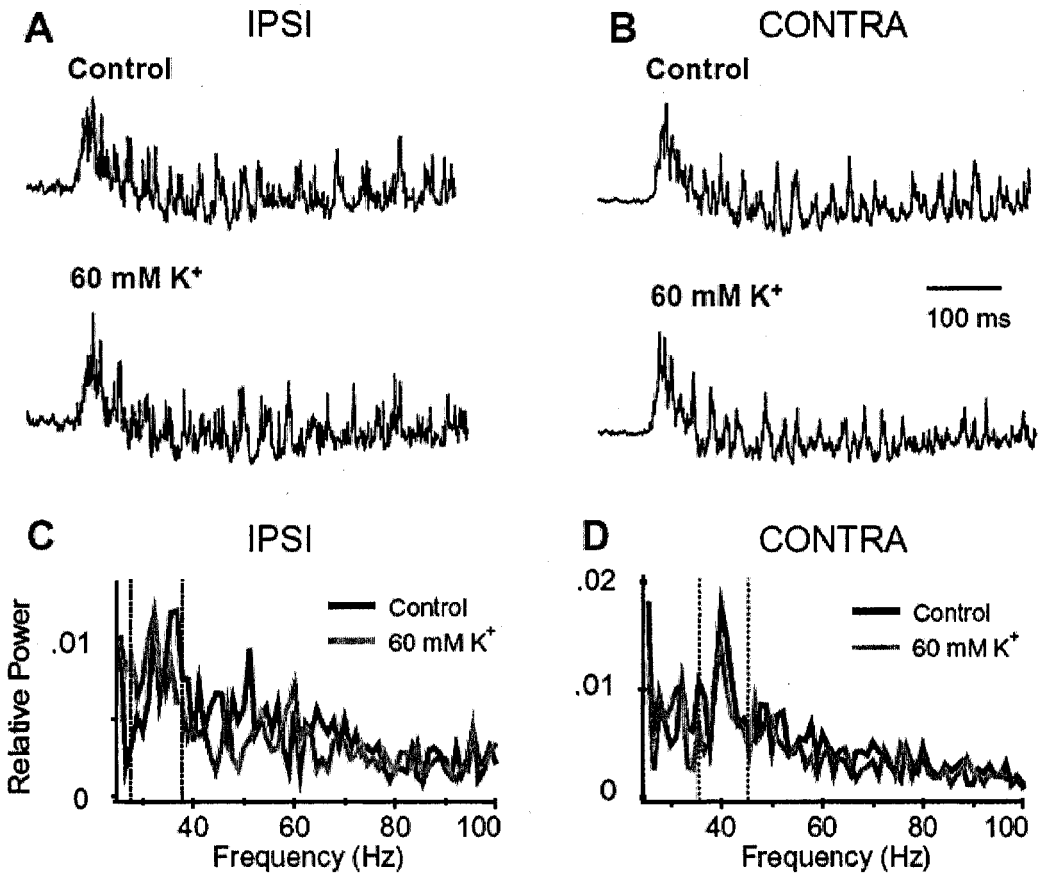

Figure 3.3: High K^+ does not increase oscillation power when unilaterally applied to the PBC. A and B. Representative raw filtered (1-200 Hz bandpass) inspiratory bursts recorded from the IPSI (A) and CONTRA (B) XII rootlet. The top traces are inspiratory bursts recorded in the control condition. The bottom traces are isnpiratory bursts recorded following local perfusion of 60 mM K^+ to the IPSI PBC. Time scale applies to all inspiratory bursts. C. Ipsilateral average relative power spectra in the control condition and following local perfusion of 60 mM K^+ to the IPSI PBC for the slice shown in A. Unilateral excitation of the PBC increases oscillation power within the bin containing the dominant peak (28-38 Hz). D. Contralateral average relative power spectra in the control condition and following local perfusion of 60 mM K^+ to the CONTRA PBC for the slice shown in B. Unilateral excitation of the PBC increases oscillation power within the bin containing the dominant peak (36-46 Hz). The bins containing the dominant peak are marked by vertical dotted lines in the IPSI and CONTRA average relative power spectra.

recorded in the control condition and the bottom traces are inspiratory bursts recorded during local perfusion of 60 mM K^+ onto the ipsilateral XII nucleus. Using the slice recordings shown in Figures 3.3A and B, the power spectra of 7 different inspiratory bursts were averaged for the left and right rootlet recordings and for each of the two conditions. The ipsilateral and contralateral average relative power spectra are shown in Figures 3.3C and D, respectively. In Figure 3.3C, the 28-38 Hz bins contain the dominant peaks for the average power spectra in control and following high K^+ application. The bin was centered around the dominant peak that reached the highest relative power value. In Figure 3.3C, the power spectrum that was computed from inspiratory bursts recorded during local perfusion of high K^+ (gray) contained the highest dominant peak at 32Hz. During unilateral local perfusion of high K^+ to the PBC, the fraction of relative power in the 28-38 Hz bins modestly increased by 5%. In Figure 3.3D, the 36-46 Hz bins contain the dominant peaks for the average power spectra in control and following high K^+ application. The bin was centered around the dominant peaks at 40Hz that are evident in power spectra computed for both conditions. During unilateral local perfusion of high K^+ to the PBC, the fraction of relative power in the 36-46 Hz bins modestly decreased by 7%.

Representative raw filtered (1-200 Hz bandpass) inspiratory bursts recorded from the ipsilateral and contralateral XII rootlets in the control condition and following unilateral local perfusion of high K^+ onto the XII nucleus are shown in Figures 3.4A and B. The top traces are inspiratory bursts recorded in the control condition and the bottom traces are inspiratory bursts recorded during local perfusion of 20 mM K^+ onto the ipsilateral XII nucleus. Using the slice recordings shown in Figures 3.4A and B, the power spectra of 14-20 different inspiratory bursts were averaged for the left and right

rootlet recordings and for each of the two conditions. The ipsilateral and contralateral average relative power spectra are shown in Figures 3.4C and D, respectively. In Figure 3.4C, the 36-46 Hz bins contain the dominant peaks for the average power

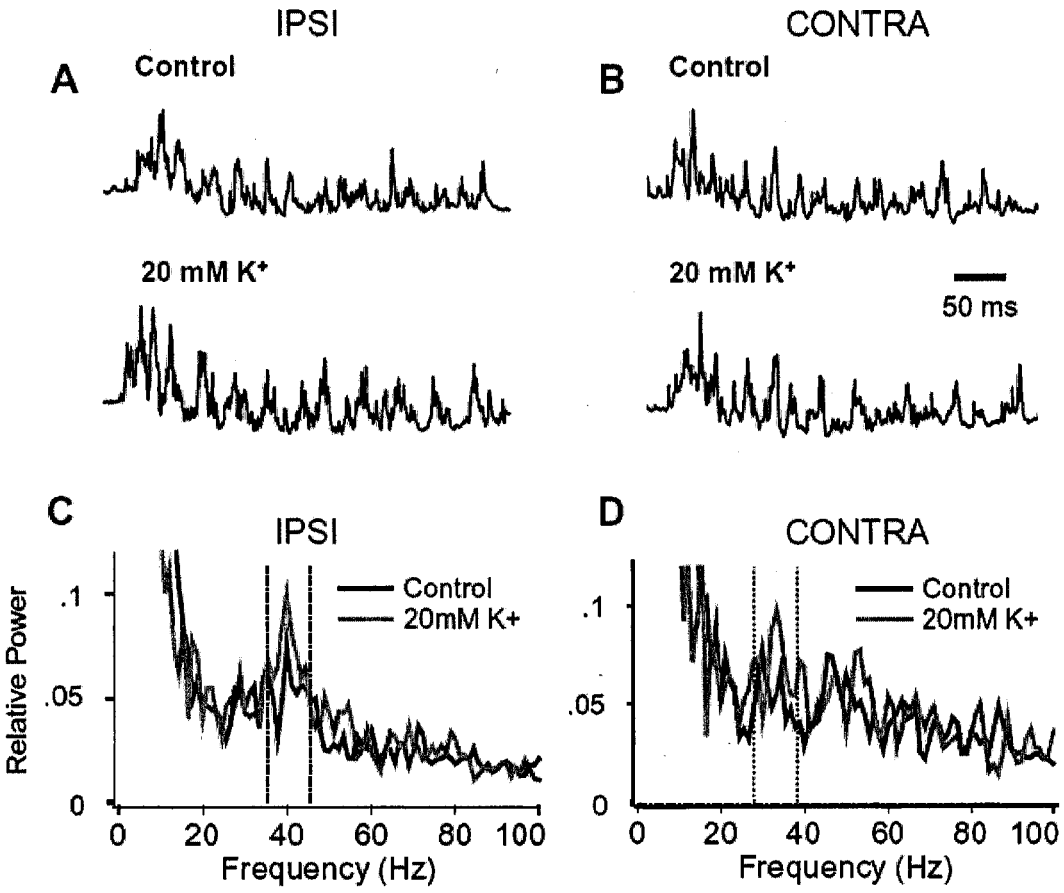

Figure 3.4: High K^+ increases oscillation power when unilaterally applied to the XII nucleus. A and B. Representative raw filtered (1-200 Hz bandpass) inspiratory bursts recorded from the IPSI (A) and CONTRA (B) XII rootlet. The top traces are inspiratory bursts recorded in the control condition. The bottom traces are isnpiratory bursts recorded following local perfusion of 20 mM K^+ to the IPSI XII nucleus. Time scale applies to all inspiratory bursts. C. Ipsilateral average relative power spectra in the control condition and following local perfusion of 20 mM K^+ to the IPSI XII nucleus. Unilateral excitation of the XII nucleus increases oscillation power within the bin containing the dominant peak (36-46 Hz). D. Contralateral average relative power spectra in the control condition and following local perfusion of 20 mM K^+ to the CONTRA XII nucleus. Unilateral excitation of the XII nucleus increases oscillation power within the bin containing the dominant peak (28-38 Hz). The bins containing the dominant peak are marked by vertical dotted lines in the IPSI and CONTRA average relative power spectra.

spectra in control and following high K^+ application. The bin was centered around the dominant peaks at 40Hz that are present in power spectra computed for both conditions. During unilateral local perfusion of high K^+ to the XII nucleus, the fraction of relative power in the 36-46 Hz bins increased by 30%. In Figure 3.4D, the 28-38 Hz bins contain the dominant peaks for the average power spectra in control and following high K^+ application. The bin was centered around the dominant peak that reached the highest relative power value. In Figure 3.4D, the power spectrum that was computed from inspiratory bursts recorded during local perfusion of high K^+ (gray) contained the highest dominant peak at 33Hz. During unilateral local perfusion of high K^+ to the XII nucleus, the fraction of relative power in the 28-38 Hz bins increased by 29%.

The summary data in Figure 3.5 show that unilateral excitation of the XII nucleus, but not the PBC, increased oscillation power unilaterally. The effect of unilateral PBC excitation on oscillation power was examined in 7 slices. For experiments in which high K^+ was unilaterally perfused onto the PBC, the effects of 60 and 80 mM K^+ on oscillation power were not different. Therefore, data from experiments using the two K^+ concentrations were pooled (n=6). Unilateral local perfusion of high K^+ to the PBC had no significant effect on oscillation power recorded from the ipsilateral (increased by 19 ± 15%, n.s.) and contralateral (increased by 52 ± 25%, n.s.) XII rootlet. Unilateral excitation of the XII nucleus significantly increased the relative power of oscillations recorded from the ipsilateral XII rootlet (by 44 ± 13%, n=8, $p<0.05$), but had no significant effect on oscillation power recorded from the contralateral XII rootlet (increased by 47 ± 25%, n=8, n.s.). Following unilateral excitation of the XII nucleus, there was no significant correlation between the percent

increase in peak integrated activity and the percent increase in the relative power of oscillations (n=8, $y = 0.06x + 41$, $r^2 = 0.003$, $p > 0.05$).

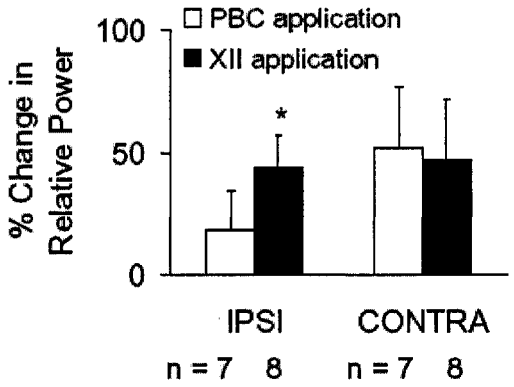

Figure 3.5: Summary of the effects of unilateral excitation of the PBC or the XII nucleus on the relative power of oscillations. Local perfusion of ACSF containing high K^+ (60 or 80 mM) to the unilateral PBC had no effect on oscillation power bilaterally. Local perfusion of ACSF containing high K^+ (20 mM) to the unilateral XII nucleus increased oscillation power in the IPSI by 44 ± 13% (n=8, $p<0.05$), but had no effect on the oscillation power recorded from the CONTRA (47 ± 25%, n=8, $p=0.15$) XII rootlet.

Although Inspiratory Motor Discharge is Crosscorrelated, Synchronous Oscillations are only Weakly Coherent

My finding that oscillation power increases in response to unilateral excitation of the XII nucleus, and not the PBC, suggests that synchronous oscillations are generated at or immediately upstream of the motoneuron level. According to our knowledge of inspiratory-phase synchronous oscillations, oscillations that are generated at the motoneuron level, which are classified as MFOs, should only be weakly coherent across left and right inspiratory nerves (Cohen et al., 1987; Christakos et al., 1991).

To investigate synchrony between the left and right XII rootlet discharge, I applied crosscorrelation and coherence analyses that reveal different forms of neural synchrony than power spectral analysis. First, crosscorrelation analysis determines

whether two signals are temporally correlated by measuring the time lag between, in this case, action potentials in the left and right XII rootlet recordings. A peak in the crosscorrelation plot would demonstrate that action potentials in the left and right XII nuclei are triggered by a common synaptic input (Sears and Stagg 1976; Kirkwood et al., 1982). Second, coherence analysis assesses whether the action potentials in the left and right XII rootlets share spectral characteristics. A sharp peak in the coherence plot, which is a hallmark of strong coherence, is evidence that oscillations in action potential firing in the left and right XII rootlets occur at the same frequency (Cohen et al., 1987). It is important to keep in mind that coherence does not require temporally correlated activity. Neurons firing at the same frequency can produce a sharp peak in the coherence plot even if their spike times are temporally uncorrelated. Therefore, crosscorrelation analysis reflects the synchrony produced by temporally correlated action potentials triggered by a common input. Coherence analysis reveals the synchrony produced when action potentials (or subthreshold changes in membrane potential) occur at the same frequency.

Crosscorrelation histograms (CCHs) of left and right XII rootlet activity recorded in the control condition demonstrated that bilaterally recorded spike firing is temporally correlated. The CCHs of left and right rootlet discharges had broad peaks (mean half amplitude width = 17.3 ± 2.1 ms, n=13) centered around an average time lag of -0.2 ± 0.6 ms. The peaks in all CCHs were statistically significant ($p<0.05$). None of the CCHs displayed harmonic peaks that arise when action potentials fire at a particular interval in a temporally correlated manner (Kirkwood et al., 1982; Christakos et al., 1991). Harmonic peaks would reflect bilaterally synchronous oscillations in spike firing that are triggered by a common synaptic input (Kirkwood et al., 1982; Christakos et al.,

1991). The two representative CCHs shown in Figure 3.6A and B reflect the characteristics common to all CCHs, those are the broad peak centered near zero and the lack of harmonic peaks.

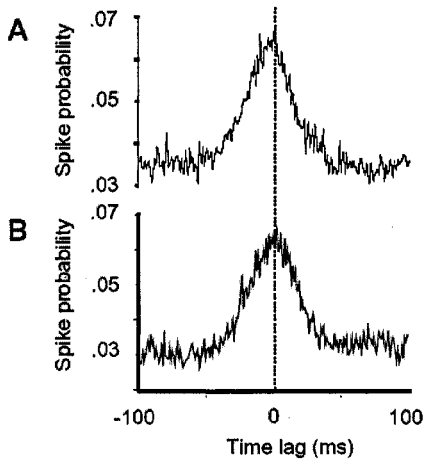

Figure 3.6: Crosscorrelation histograms (CCHs) of left and right hypoglossal rootlet activity produce broad peaks centered around a time lag of zero and no harmonic peaks. Representative CCHs from P4 and P5 mice are shown in (A) and (B), respectively. In (A), the peak occurs at -1 ms and has a half width of 20.5 ms. In (B), the peak occurs at 2 ms and has a half width of 20.5 ms. For both CCHs, the bin width equals 1 ms. Dashed vertical line marks zero time lag.

Next, I compared the half amplitude widths, time lag of the peaks, and the spike probability in the peak region for CCHs computed from left and right XII rootlet activity recorded in the control condition and following local perfusion of high K^+. Unilateral high K^+ application to the PBC did not change the half amplitude widths (decreased by -0.06 ± 0.14 %, n=5, n.s.; control: 14.0 ± 4.6 ms, high K^+: 13.4 ± 5.0 ms), the time lag of the peaks (control: -1.0 ± 1.3 ms, high K^+: 0.4 ± 0.7 ms, n=5), or introduce harmonic peaks to the CCHs. Likewise, unilateral high K^+ application to the XII did not change the half amplitude widths (decreased by –0.1 ± 0.19 %, n=8, n.s.; control: 19.4 ± 1.7 ms, high K^+: 16.4 ± 3.1 ms), the time lag of the peaks (control: 0.3 ± 0.7 ms, high K^+:

-0.6 ± 0.6 ms, n=8), or introduce harmonic peaks to the CCHs. Unilateral high K^+ application to the XII nucleus significantly increased the spike firing probability in the peak region of the CCHs by 44 ± 27 % (n=8, $p<0.05$; spike firing probability in control: 0.05 ± 0.007, spike firing probability in high K^+: 0.07 ± 0.006 ms). This increase is explained by the bilateral increase in peak integrated activity following unilateral excitation of the XII nucleus and does not reflect an increase in the strength of synchronization. In contrast, unilateral excitation of the PBC did not affect spike firing probability in the peak region of the CCHs (decreased by -1 ± 7 %, n=5, n.s.; spike firing probability in control: 0.07 ± 0.008, spike firing probability in high K^+: 0.07 ± 0.006 ms). Following unilateral excitation of the PBC (n=5) and the XII nucleus (n=8), the central peaks in the CCHs remained statistically significant ($p<0.05$).

Coherence plots were computed using the left and right average relative power spectra for 8 pairs of XII rootlets. None of the coherence plots displayed the sharp, significant peaks that are characteristic of strong HFO associated coherence (Cohen et al., 1997). Instead all of the plots showed only weak, but significant coherence reflected by many small peaks that rose above the upper 95% confidence limit. Figures 3.7A and B show the representative left and right average absolute power respectively, used to compute the representative coherence plot in Figure 3.7C. Dominant peaks in the left and right average absolute power spectra occur at 39 and 36 Hz (dashed vertical lines), respectively. In the corresponding coherence plot, 36 and 39 Hz are marked by the two dashed vertical lines and the upper 95% confidence limit is marked by the dashed horizontal line. Coherence is not significant at 36 Hz, but is just above the confidence limit at 39 Hz. Weak coherence is reflected by the many small peaks between 38 and 72 Hz that rise above the confidence limit, however, there is no

dominant peak. The broad coherence peak that appears on the left side of the x-axis reflects the coherence due to the lower frequency envelope of the inspiratory burst.

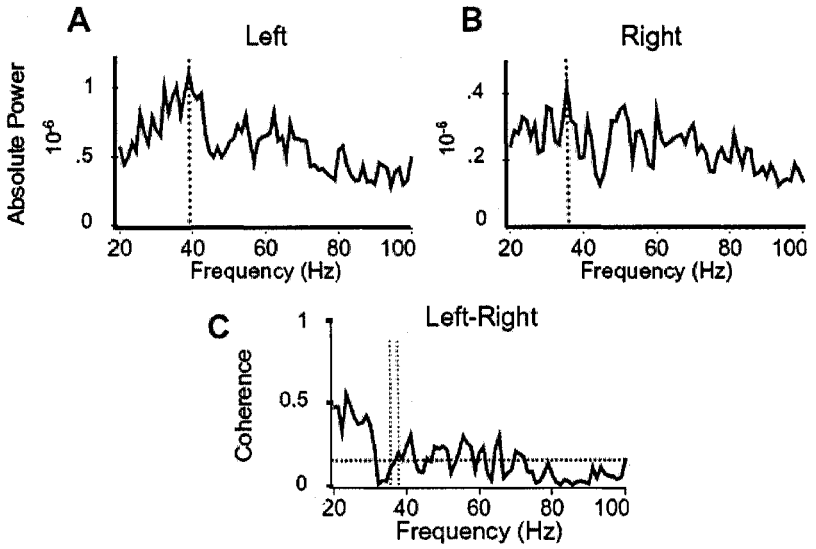

Figure 3.7: Bilaterally recorded synchronous oscillations are weakly coherent. A and B. Left and right average absolute power spectra each computed from 20 inspiratory bursts recorded in the control condition. Dashed vertical lines mark the location of the dominant peaks in the left and right power spectra at 39 and 36 Hz, respectively. C. Coherence plot computed from the left and right average absolute power spectra in A and B. The dashed horizontal line marks the upper 95% confidence limit at 0.145. 36 and 39 Hz are marked by the two dashed vertical lines. Although there are peaks in the left (A) and right (B) average absolute power spectra at 39 and 36 Hz, respectively, the oscillations are only weakly coherent at these frequencies. The peak less than 35 Hz reflects the coherence due to the envelope of the inspiratory burst that occurs in a low frequency range.

For each coherence plot computed for the control condition and following unilateral local perfusion of high K^+, I measured the statistically significant coherence from 0-100 Hz. The statistically significant coherence is defined as the coherence greater than the upper 95% confidence limit (see Methods). Unilateral excitation of the PBC had no effect on significant coherence from 0-100 Hz (15 ± 10%, n=4, n.s.; control: 8.9 ± 2.0; unilateral PBC excitation: 10.4 ± 2.6). Unilateral excitation of the XII

nucleus also had no effect on significant coherence from 0-100 Hz (33 ± 49%, n=4, n.s.; control: 12.1 ± 3.4; unilateral PBC excitation: 11.2 ± 1.6). Therefore, neither unilateral excitation of the PBC nor the XII nucleus affected the coherence of oscillations recorded from the ipsilateral and contralateral XII rootlets.

Discussion

In this chapter, I examined long and short time scale synchrony in the inspiratory network by unilaterally exciting either the PBC or the XII nucleus while bilaterally recording inspiratory motor outflow. The principal findings of this work are twofold. First, I demonstrated that unilateral excitation of the PBC versus the XII nucleus has differential effects on inspiratory activity recorded bilaterally. Second, based on the results from local perfusion experiments and coherence analysis I concluded that synchronous oscillations exhibited by the rhythmically active slice preparation are MFOs that are generated at or near the level of the XII motor nucleus.

Increasing Excitability in the PBC versus the XII Nucleus has Differential Effects on Inspiratory Activity

Local application of high K^+ to the PBC versus the XII nucleus has differential effects on mean inspiratory burst frequency and mean peak integrated activity both of which are measures of long time scale synchrony. Local perfusion of high K^+ onto the PBC increased mean inspiratory burst frequency bilaterally, but had no effect on mean peak integrated activity. In contrast, local perfusion of high K^+ onto the XII nucleus had no effect on inspiratory burst frequency but bilaterally increased mean peak integrated activity. These two findings are consistent with previous work in which the excitability of

the PBC or the XII has been modulated bilaterally (Smith et al., 1991; Funk et al., 1993).

When the rhythmically active medullary slice preparation was first introduced, Smith et al. demonstrated that microinjection of high K^+ to the unilateral PBC increased inspiratory burst frequency bilaterally in a reversible manner (Smith et al., 1991). As expected, unilaterally reducing excitability in the PBC had the converse effect on inspiratory burst frequency (Smith et al., 1991; Funk et al., 1993). Microinjection of a non-NMDAR antagonist onto the unilateral PBC reduced inspiratory burst frequency recorded from the left and right XII rootlets without affecting peak integrated activity. Funk et al. (1993) also blocked non-NMDARs in the unilateral XII nucleus and found that reducing the excitability of the XII nucleus reduced the peak amplitude of inspiratory bursts bilaterally but had no effect on inspiratory burst frequency.

These previously reported findings and the present work demonstrate that modulating the excitability of the PBC versus the XII nucleus has differential effects on inspiratory burst frequency and peak integrated activity. These results are consistent with the properties and functions of neurons in the PBC and XII nucleus. Pacemaker neurons in the PBC generate inspiratory rhythm and produce a faster inspiratory burst frequency when they are depolarized (Butera, Jr. et al., 1999; Del Negro et al., 2001). HMs transmit inspiratory rhythm to inspiratory tongue muscles and are involved in modulating the gain of inspiratory-phase discharge (Funk et al., 1993; Yasuda et al., 2001).

Connections Mediating Bilateral Synchrony

The bilateral increase in inspiratory burst frequency following unilateral excitation of the PBC confirms that activity in the left and right PBCs are synaptically linked. Calcium imaging of the rhythmic slice preparation has demonstrated that glutamatergic connections between the left and right PBCs synchronize PBC inspiratory activity bilaterally (Koshiya and Smith 1999).

I also found that unilateral excitation of the XII nucleus increased peak integrated activity recorded bilaterally. These data are consistent with previous work in which Funk et al. (1993) reported that microinjection of non-NMDAR antagonists to the unilateral XII nucleus bilaterally decreased inspiratory burst amplitudes recorded from the XII rootlets (Funk et al., 1993). Nevertheless, I cannot rule out the possibility that some of the high K^+ that I locally perfused onto the unilateral XII nucleus diffused to the contralateral XII nucleus. However, the direction of the bath perfusate was parallel to the direction of the local perfusate and the local perfusate was suctioned off the tissue as soon as it passed over the unilateral XII nucleus. For the local perfusate to spread to the contralateral XII nucleus, it would have had to diffuse against the direction of flow of the bath.

Alternatively, the observed bilateral increase in mean peak integrated activity following unilateral excitation of the XII nucleus may be explained by two cellular mechanisms. First, unilateral application of high K^+ to the XII nucleus may activate midline crossing dendrites that originate from contralateral HMs and trigger spike firing in HMs located in the contralateral motor nucleus. Neurobiotin labeling of individual rat HMs during postnatal development showed that HM dendrites project radially from the soma with some dendritic processes crossing the midline and projecting into the

contralateral XII nucleus (Nunez-Abades et al., 1994). Second, unilateral excitation of the XII nucleus may increase spike firing bilaterally if some ipsilateral and contralateral HMs are electrically coupled. A combination of biochemical, immunohistochemical (Solomon 2003) and electrophysiological studies (Bou-Flores and Berger 2001; Solomon et al., 2003) provide strong evidence that gap junction proteins are present in the neonatal and adult inspiratory network and can modulate inspiratory motoneuron synchronization. Dendrodendritic or dendrosomatic gap junctions would explain the tracer coupling between neonatal HMs located in the ipsilateral and contralateral XII nuclei (Mazza et al., 1992). Therefore, it is possible that dendrites from one XII nucleus cross the midline and form chemical or electrical synapses with HMs on the contralateral side. Such chemical or electrical coupling between ipsilateral and contralateral HMs may underlie modest synchrony between the left and right XII nuclei.

Inspiratory Motor Discharge is Bilaterally Synchronized on a Long Time Scale, but Not on a Short Time Scale

By applying crosscorrelation analysis to bilaterally recorded inspiratory activity, the present work demonstrates that action potentials between the left and right XII rootlet discharges are temporally correlated on a long time scale. However, the absence of harmonic peaks in the CCHs and the lack of strong coherence demonstrate that oscillations recorded from the left and right XII rootlets in the slice are not temporally correlated and do not occur at the same frequency, respectively. As such, inspiratory phase synchronous oscillations recorded from the slice are MFOs that are likely generated at or immediately upstream of the XII nucleus.

Each CCH of left and right XII rootlet discharge was characterized by a broad peak centered near a time lag of zero. This broad peak is also a common feature of CCHs that have been computed from inspiratory neural activity such as that recorded from two inspiratory neurons (Kirkwood et al., 1982; Kashiwagi et al., 1993) and multiunit activity recorded bilaterally from the XII nuclei (Li et al., 2003). A peak in the CCH centered near a time lag of zero demonstrates that the neural discharges are synchronized by a common input. The broadness of the peak reflects the variability in the time lag produced by a polysynaptic connection between the source of common input and the recording site (Kirkwood et al., 1982). In the rhythmically active slice preparation, the left and right XII rootlet discharges are likely synchronized by the bilaterally connected PBCs. Given the broad peak in each CCH, I believe that PBC neurons transmit inspiratory rhythm to HMs via a polysynaptic input. Although the circuitry between the PBC and the XII nucleus is still unknown, PBC neurons likely transmit inspiratory rhythm to the XII nucleus via a polysynaptic pathway which involves premotoneurons (Dobbins and Feldman 1995; Li et al., 1997; Ezure and Tanaka 2006).

Although spike firing between the left and right XII rootlet recordings are temporally correlated on a long time scale, the CCHs and coherence plots presented here provide strong evidence that inspiratory motor discharge is not bilaterally synchronized on a short time scale *in vitro*. If action potentials in the bilateral XII rootlet activity are temporally correlated and occur within the same frequency range, the central peak in each CCH would be flanked by harmonic peaks and the cycle time of each harmonic peak would correspond to the cycle time of a single synchronous oscillation (Kirkwood et al., 1982; Cohen et al., 1987; Christakos et al., 1991). Such harmonic peaks are characteristic of CCHs computed from neural activity exhibiting

HFOs that are generated and synchronized via a common input source. None of the CCHs computed in this study exhibit harmonic peaks. This suggests that synchronous oscillations recorded from the left and right XII rootlets *in vitro* are MFOs that generated individually in or immediately upstream of the XII nucleus.

This conclusion is further supported by the results of coherence analysis. If the bilateral rootlet recordings exhibited oscillations occurring at the same frequency but were not necessarily temporally coincident, then the coherence plots should display a prominent and significant peak which is characteristic of HFOs. None of the coherence plots showed such a peak suggesting that bilaterally recorded synchronous oscillations do not occur at the same frequency and can therefore be categorized as MFOs.

The broad peak and absence of harmonic peaks in the CCHs, and the absence of strong coherence support my conclusion that inspiratory XII rootlet discharge is bilaterally synchronized on a long time scale but not on a short time scale. Given that oscillations recorded from the left and right XII rootlets are not temporally coincident and do not occur at the same frequency, they can be categorized as MFOs (Cohen et al., 1987; Christakos et al., 1991) and are likely generated in or immediately upstream of the XII nucleus.

Origin of Synchronous Oscillations in the Rhythmic Slice

The principal aim of the present study was to determine where in the rhythmically active slice preparation synchronous oscillations are generated. Together, the data from local application experiments and crosscorrelation and coherence analyses demonstrate that synchronous oscillations in the slice are MFOs that are generated in the XII nucleus or immediately upstream of the XII nucleus in the premotor

area. Upon consideration of the cellular architecture necessary to generate synchronous oscillations, I conclude that the XII nucleus is not equipped to generate synchronous oscillations and that oscillations are likely to be generated in the premotor area.

The PBC is thought to propagate inspiratory rhythm to multiple motor pools, including the XII nucleus, via premotoneurons that are located in an intermediate zone between the PBC and the motor nuclei. Premotoneurons that project to the HMs are located lateral and ventrolateral to the hypoglossal nucleus (Dobbins and Feldman 1995) and some of these premotoneurons are GABAergic or glycinergic (Li et al., 1997). A premotor origin for synchronous oscillations is consistent with the increase in relative power produced by excitation of the XII nucleus. If oscillations are generated in the premotor area, HMs would receive oscillatory synaptic inputs from premotor neurons. Depolarizing the resting membrane potential of HMs, by locally perfusing high K^+ onto the XII nucleus, would increase their probability of firing action potentials in response to the oscillatory inputs and thereby increase the computed oscillation power.

Although the increase in relative power following unilateral excitation of the XII nucleus can be explained by a motor origin for synchronous oscillations, neurons in the XII nucleus lack the cellular morphology and synaptic properties necessary to generate synchronous oscillations. In Chapter 2, I demonstrated that GABAergic and glycinergic transmission are required to generate synchronous oscillations. Further, I proposed a model, based on studies in the hippocampus (Cobb et al., 1995; Fisahn et al., 1998) and olfactory bulb (Schoppa 2006), in which alternating excitatory and inhibitory inputs as well as recurrent axon collaterals are required to generate inspiratory-phase synchronous oscillations. The XII nucleus is ill-equipped to generate synchronous

oscillations in that HMs lack recurrent axon collaterals and interneurons within the XII nucleus that could provide inhibitory synaptic inputs are scarce (Viana et al., 1990). Therefore, oscillations are more likely to be generated in the premotor area, which contains both excitatory and inhibitory neurons (Li et al., 1997), and transmitted to the XII nucleus.

Despite the potential importance of premotoneurons in generating synchronous oscillations, transmitting inspiratory activity to inspiratory motoneurons and in modulating inspiratory rhythm, relatively little is known about this region. In the future, it will be interesting to identify the location of the premotor area and to characterize the properties of premotor neurons. This information will have important implications with respect to understanding how inspiratory rhythm is transmitted and modulated before it reaches the XII nucleus and, possibly, how synchronous oscillations are generated in the premotor area.

Chapter 4: General Conclusions and Future Directions

The brainstem respiratory network serves as an excellent model with which to study long time scale, short time scale and bilateral synchrony because all three forms of synchrony are exhibited during inspiration. By recording bilateral inspiratory activity from the XII rootlets of the rhythmically active slice preparation, I was able to investigate all three forms synchrony. However, my thesis research was directed toward answering questions regarding how inspiratory-phase short time scale synchrony is generated and where synchronous oscillations are produced. I can make four general conclusions with respect to the development, generation and origin of inspiratory-phase synchronous oscillations. First, I have shown that synchronous oscillation frequency increases during postnatal development. Although there are many changes in the inspiratory network that occur during postnatal development, one change that may explain an increase in oscillation frequency is the shortening in the decay time course of GABAergic and glycinergic currents that is known to occur. Second, I have demonstrated that GABAergic and glycinergic transmission are required to generate robust synchronous oscillations during postnatal development. Third, by prolonging the decay time course of GABAergic currents, I demonstrated that the time course of inhibitory currents is a determinant of oscillation frequency. Therefore, it is likely that synchronous oscillations are generated by recurrent synaptic connections between excitatory and inhibitory neurons that produce the clusters of action potentials that are separated by periods of little or no activity (Figure 1.3). This model for the generation of synchronous oscillations is supported by previous work in other neural systems, namely the hippocampus and olfactory bulb (Cobb et al., 1995; Fisahn et al., 1998; Schoppa

2006). Lastly, by integrating data from local application experiments and crosscorrelation and coherence analysis, I conclude that inspiratory-phase synchronous oscillations are likely MFOs that are generated in the premotor area. The premotor area remains a region about which little is known yet its intermediate location between the PBC and the XII nucleus suggests that it plays an important role in transmitting inspiratory rhythm from inspiratory pacemaker neurons to inspiratory motoneurons and in modulating inspiratory rhythm. Now, data presented in Chapter 3 implicate the premotor area as the origin of MFOs recorded from the XII rootlets in the rhythmically active slice preparation. As yet, we know that premotoneurons that project to the hypoglossal nucleus are located lateral and ventrolateral to the XII nucleus. Further, some premotoneurons that project to the XII nucleus are GABAergic or glycinergic (Li et al., 1997; Ezure and Tanaka 2006).

In a number of additional experiments, I have used a field electrode to probe the area between the PBC and the XII nucleus and have been able to locate a potential premotor area in a single slice. In this slice, the potential premotor area was located in a confined region ~1 mm dorsomedial to the PBC and ~1.5 mm ventrolateral to the XII nucleus. This region exhibited inspiratory activity in phase with the inspiratory rhythm recorded from the XII rootlet (Figure 4.1). In future experiments, it will be of great interest to electrophysiologically identify the location of the premotor area within the brainstem, characterize the electrophysiological properties of premotor neurons and determine the types of synaptic inputs (e.g. glutamatergic, GABAergic and glycinergic) premotor neurons receive and transmit.. After the location of the premotor area is identified, it will be easier to find and record from premotor neurons and to characterize their electrophysiological and synaptic properties. It would be particularly interesting to

determine whether the premotor area contains GABAergic neurons that may be involved in generating synchronous oscillations. With respect to inspiratory activity, GABAergic premotor neurons may be the source of GABAergic inputs that HMs receive during inspiration and that shape the pattern of inspiratory discharge (Saywell and Feldman 2004). By elucidating the location and properties of premotor neurons, we would make significant progress toward understanding how inspiratory rhythm is transmitted from pacemaker neurons to inspiratory motoneurons and the synaptic connections that produce inspiratory-phase synchronous oscillations.

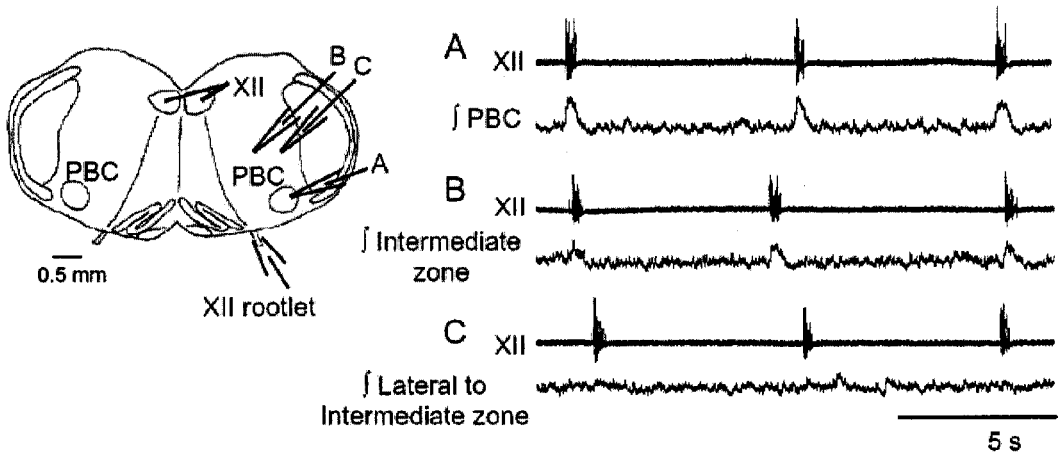

Figure 4.1: The premotor area is located in an intermediate zone between the PBC and XII nucleus. While recording inspiratory rhythm from the XII rootlet, using the rhythmic slice preparation, I sequentially placed a field electrode on the PBC (A), on an intermediate zone between the PBC and the XII nucleus (B), and 500 μm lateral to the intermediate zone (C). On the right, are three pairs of traces showing inspiratory rhythm recorded from the XII rootlet and activity recorded from either the PBC (A), the intermediate zone (B), or a region just lateral to the intermediate zone. The proposed premotor area is confined to an intermediate zone located ~ 1mm dorsomedial to the PBC and ~1.5mm ventrolateral to the XII nucleus. Inspiratory rhythm was not detected in the region 500 μm lateral to the intermediate zone.

References

Baker MR and Baker SN. The effect of diazepam on motor cortical oscillations and corticomuscular coherence studied in man. *J Physiol* 546: 931-942, 2003.

Baker SN, Kilner JM, Pinches EM and Lemon RN. The role of synchrony and oscillations in the motor output. *Exp Brain Res* 128: 109-117, 1999.

Bou-Flores C and Berger AJ. Gap junctions and inhibitory synapses modulate inspiratory motoneuron synchronization. *J Neurophysiol* 85: 1543-1551, 2001.

Busselberg D, Bischoff AM, Paton JF and Richter DW. Reorganisation of respiratory network activity after loss of glycinergic inhibition. *Pflugers Arch* 441: 444-449, 2001.

Butera RJ, Jr., Rinzel J and Smith JC. Models of respiratory rhythm generation in the pre-Botzinger complex. II. Populations Of coupled pacemaker neurons. *J Neurophysiol* 82: 398-415, 1999.

Cherubini E, Gaiarsa JL and Ben Ari Y. GABA: an excitatory transmitter in early postnatal life. *Trends Neurosci* 14: 515-519, 1991.

Christakos CN, Cohen MI, Barnhardt R and Shaw CF. Fast rhythms in phrenic motoneuron and nerve discharges. *J Neurophysiol* 66: 674-687, 1991.

Cobb SR, Buhl EH, Halasy K, Paulsen O and Somogyi P. Synchronization of neuronal activity in hippocampus by individual GABAergic interneurons. *Nature* 378: 75-78, 1995.

Cohen MI. Synchronization of discharge, spontaneous and evoked, between inspiratory neurons. *Acta Neurobiol Exp (Wars)* 33: 189-218, 1973.

Cohen MI, Huang W, See WR, Yu Q and Christakos CN. Fast Rhythms in Respiratory Neural Activities. In: Neural Control of Respiratory Muscles, edited by Miller AD, Bianchi AL and Bishop BP. Boca Raton: CRC Press, 1997, p. 159-169.

Cohen MI, Piercey MF, Gootman PM and Wolotsky P. Synaptic connections between medullary inspiratory neurons and phrenic motoneurons as revealed by cross-correlation. *Brain Res* 81: 319-324, 1974.

Cohen MI, See WR, Christakos CN and Sica AL. High-frequency and medium-frequency components of different inspiratory nerve discharges and their modification by various inputs. *Brain Res* 417: 148-152, 1987.

Del Negro CA, Johnson SM, Butera RJ and Smith JC. Models of respiratory rhythm generation in the pre-Botzinger complex. III. Experimental tests of model predictions. *J Neurophysiol* 86: 59-74, 2001.

Del Negro CA, Koshiya N, Butera RJ, Jr. and Smith JC. Persistent sodium current, membrane properties and bursting behavior of pre-botzinger complex inspiratory neurons in vitro. *J Neurophysiol* 88: 2242-2250, 2002.

Del Negro CA, Morgado-Valle C, Hayes JA, Mackay DD, Pace RW, Crowder EA and Feldman JL. Sodium and calcium current-mediated pacemaker neurons and respiratory rhythm generation. *J Neurosci* 25: 446-453, 2005.

Dittler R and Garten S. Die zeitliche folge der aktionsstrome in phrenicus und zwerchfell bei der naturlichen innervation. *Zeitshrift fur Biologie* 58: 420-450, 1912.

Dobbins EG and Feldman JL. Differential innervation of protruder and retractor muscles of the tongue in rat. *J Comp Neurol* 357: 376-394, 1995.

Ezure K and Tanaka I. Distribution and medullary projection of respiratory neurons in the dorsolateral pons of the rat. *Neuroscience* 141: 1011-1023, 2006.

Fisahn A, Pike FG, Buhl EH and Paulsen O. Cholinergic induction of network oscillations at 40 Hz in the hippocampus in vitro. *Nature* 394: 186-189, 1998.

Funk GD and Parkis MA. High frequency oscillations in respiratory networks: functionally significant or phenomenological? *Respir Physiol Neurobiol* 131: 101-120, 2002.

Funk GD, Smith JC and Feldman JL. Generation and transmission of respiratory oscillations in medullary slices: role of excitatory amino acids. *J Neurophysiol* 70: 1497-1515, 1993.

Gelperin A. Olfactory computations and network oscillation. *J Neurosci* 26: 1663-1668, 2006.

Goldstein PA, Elsen FP, Ying SW, Ferguson C, Homanics GE and Harrison NL. Prolongation of hippocampal miniature inhibitory postsynaptic currents in mice lacking the GABA(A) receptor alpha1 subunit. *J Neurophysiol* 88: 3208-3217, 2002.

Graham K and Duffin J. Cross correlation of medullary expiratory neurons in the cat. *Exp Neurol* 73: 451-464, 1981.

Gray PA, Rekling JC, Bocchiaro CM and Feldman JL. Modulation of respiratory frequency by peptidergic input to rhythmogenic neurons in the preBotzinger complex. *Science* 286: 1566-1568, 1999.

Halliday DM and Rosenberg JR. Time and Frequency Domain Analysis of Spike Train and Time Series Data. In: Modern Techniques in Neuroscience Research, edited by Windhorst U and Johansson H. Berlin: Springer, 2006, p. 503-543.

Hayashi F and Lipski J. The role of inhibitory amino acids in control of respiratory motor output in an arterially perfused rat. *Respir Physiol* 89: 47-63, 1992.

Hlastala MP and Berger AJ. *Physiology of Respiration.* Oxford University Press, 2001.

Hormuzdi SG, Pais I, LeBeau FE, Towers SK, Rozov A, Buhl EH, Whittington MA and Monyer H. Impaired electrical signaling disrupts gamma frequency oscillations in connexin 36-deficient mice. *Neuron* 31: 487-495, 2001.

Janczewski WA and Feldman JL. Distinct rhythm generators for inspiration and expiration in the juvenile rat. *J Physiol* 570: 407-420, 2006.

Johnson SM, Koshiya N and Smith JC. Isolation of the kernel for respiratory rhythm generation in a novel preparation: the pre-Botzinger complex "island". *J Neurophysiol* 85: 1772-1776, 2001.

Johnson SM, Wilkerson JE, Wenninger MR, Henderson DR and Mitchell GS. Role of synaptic inhibition in turtle respiratory rhythm generation. *J Physiol* 544: 253-265, 2002.

Kahana MJ. The cognitive correlates of human brain oscillations. *J Neurosci* 26: 1669-1672, 2006.

Kandler K and Gillespie DC. Developmental refinement of inhibitory sound-localization circuits. *Trends Neurosci* 28: 290-296, 2005.

Kashiwagi M, Onimaru H and Homma I. Correlation analysis of respiratory neuron activity in ventrolateral medulla of brainstem-spinal cord preparation isolated from newborn rat. *Exp Brain Res* 95: 277-290, 1993.

Khawaled R, Bruening-Wright A, Adelman JP and Maylie J. Bicuculline block of small-conductance calcium-activated potassium channels. *Pflugers Arch* 438: 314-321, 1999.

Kirkwood PA, Sears TA, Tuck DL and Westgaard RH. Variations in the time course of the synchronization of intercostal motoneurones in the cat. *J Physiol* 327: 105-135, 1982.

Kocsis B, Gyimesi-Pelczer K and Vertes RP. Medium-frequency oscillations dominate the inspiratory nerve discharge of anesthetized newborn rats. *Brain Res* 818: 180-183, 1999.

Koshiya N and Guyenet PG. Tonic sympathetic chemoreflex after blockade of respiratory rhythmogenesis in the rat. *J Physiol* 491 (Pt 3): 859-869, 1996.

Koshiya N and Smith JC. Neuronal pacemaker for breathing visualized in vitro. *Nature* 400: 360-363, 1999.

Kuwana S, Tsunekawa N, Yanagawa Y, Okada Y, Kuribayashi J and Obata K. Electrophysiological and morphological characteristics of GABAergic respiratory neurons in the mouse pre-Botzinger complex. *Eur J Neurosci* 23: 667-674, 2006.

Li YM, Shen L, Peever JH and Duffin J. Connections between respiratory neurones in the neonatal rat transverse medullary slice studied with cross-correlation. *J Physiol* 549: 327-332, 2003.

Li YQ, Takada M, Kaneko T and Mizuno N. Distribution of GABAergic and glycinergic premotor neurons projecting to the facial and hypoglossal nuclei in the rat. *J Comp Neurol* 378: 283-294, 1997.

Lieske SP, Thoby-Brisson M, Telgkamp P and Ramirez JM. Reconfiguration of the neural network controlling multiple breathing patterns: eupnea, sighs and gasps [see comment]. *Nat Neurosci* 3: 600-607, 2000.

Liu G, Feldman JL and Smith JC. Excitatory amino acid-mediated transmission of inspiratory drive to phrenic motoneurons. *J Neurophysiol* 64: 423-436, 1990.

Liu Q and Wong-Riley MT. Postnatal expression of neurotransmitters, receptors, and cytochrome oxidase in the rat pre-Botzinger complex. *J Appl Physiol* 92: 923-934, 2002.

Liu Q and Wong-Riley MT. Developmental changes in the expression of GABAA receptor subunits alpha1, alpha2, and alpha3 in the rat pre-Botzinger complex. *J Appl Physiol* 96: 1825-1831, 2004.

Liu Q and Wong-Riley MT. Postnatal developmental expressions of neurotransmitters and receptors in various brain stem nuclei of rats. *J Appl Physiol* 98: 1442-1457, 2005.

MacLeod K and Laurent G. Distinct mechanisms for synchronization and temporal patterning of odor-encoding neural assemblies. *Science* 274: 976-979, 1996.

Mann EO, Radcliffe CA and Paulsen O. Hippocampal gamma-frequency oscillations: from interneurones to pyramidal cells, and back. *J Physiol* 562: 55-63, 2005.

Marchetti C, Pagnotta S, Donato R and Nistri A. Inhibition of spinal or hypoglossal motoneurons of the newborn rat by glycine or GABA. *Eur J Neurosci* 15: 975-983, 2002.

Mazza E, Nunez-Abades PA, Spielmann JM and Cameron WE. Anatomical and electrotonic coupling in developing genioglossal motoneurons of the rat. *Brain Res* 598: 127-137, 1992.

Mellen NM, Janczewski WA, Bocchiaro CM and Feldman JL. Opioid-induced quantal slowing reveals dual networks for respiratory rhythm generation. *Neuron* 37: 821-826, 2003.

Mitchell RA and Herbert DA. Synchronized high frequency synaptic potentials in medullary respiratory neurons. *Brain Res* 75: 350-355, 1974.

Moore DS and McCabe GP. Introduction to Inference. In: Introduction to the Practice of Statistics, New York: W.H. Freeman and Company, 1999, p. 433-501.

Nordstrom MA, Fuglevand AJ and Enoka RM. Estimating the strength of common input to human motoneurons from the cross-correlogram. *J Physiol* 453: 547-574, 1992.

Nunez-Abades PA, He F, Barrionuevo G and Cameron WE. Morphology of developing rat genioglossal motoneurons studied in vitro: changes in length, branching pattern, and spatial distribution of dendrites. *J Comp Neurol* 339: 401-420, 1994.

O'Neal MH, III, Spiegel ET, Chon KH and Solomon IC. Time-frequency representation of inspiratory motor output in anesthetized C57BL/6 mice in vivo. *J Neurophysiol* 93: 1762-1775, 2005.

Onimaru H, Kumagawa Y and Homma I. Respiration-related rhythmic activity in the rostral medulla of newborn rats. *J Neurophysiol* 96: 55-61, 2006.

Palva JM, Lamsa K, Lauri SE, Rauvala H, Kaila K and Taira T. Fast network oscillations in the newborn rat hippocampus in vitro. *J Neurosci* 20: 1170-1178, 2000.

Parkis MA, Feldman JL, Robinson DM and Funk GD. Oscillations in endogenous inputs to neurons affect excitability and signal processing. *J Neurosci* 23: 8152-8158, 2003.

Paton JF and Richter DW. Maturational changes in the respiratory rhythm generator of the mouse. *Pflugers Arch* 430: 115-124, 1995a.

Paton JF and Richter DW. Role of fast inhibitory synaptic mechanisms in respiratory rhythm generation in the maturing mouse. *J Physiol* 484 (Pt 2): 505-521, 1995b.

Pauluis Q, Baker SN and Olivier E. Emergent oscillations in a realistic network: the role of inhibition and the effect of the spatiotemporal distribution of the input. *J Comput Neurosci* 6: 27-48, 1999.

Peever JH and Duffin J. Bilateral synchronisation of respiratory motor output in rats: adult versus neonatal in vitro preparations. *Pflugers Arch* 442: 943-951, 2001.

Peever JH, Shen L and Duffin J. Respiratory pre-motor control of hypoglossal motoneurons in the rat. *Neuroscience* 110: 711-722, 2002.

Pena F, Parkis MA, Tryba AK and Ramirez JM. Differential contribution of pacemaker properties to the generation of respiratory rhythms during normoxia and hypoxia. *Neuron* 43: 105-117, 2004.

Pierrefiche O, Schwarzacher SW, Bischoff AM and Richter DW. Blockade of synaptic inhibition within the pre-Botzinger complex in the cat suppresses respiratory rhythm generation in vivo. *J Physiol* 509 (Pt 1): 245-254, 1998.

Ramirez JM, Quellmalz UJ and Richter DW. Postnatal changes in the mammalian respiratory network as revealed by the transverse brainstem slice of mice. *J Physiol* 491 (Pt 3): 799-812, 1996.

Ramirez JM, Zuperku EJ, Alheid GF, Lieske SP, Ptak K and McCrimmon DR. Respiratory rhythm generation: converging concepts from in vitro and in vivo approaches? *Respir Physiol Neurobiol* 131: 43-56, 2002.

Rekling JC, Funk GD, Bayliss DA, Dong XW and Feldman JL. Synaptic control of motoneuronal excitability. *Physiol Rev* 80: 767-852, 2000.

Ren J and Greer JJ. Modulation of respiratory rhythmogenesis by chloride-mediated conductances during the perinatal period. *J Neurosci* 26: 3721-3730, 2006.

Richardson CA and Mitchell RA. Power spectral analysis of inspiratory nerve activity in the decerebrate cat. *Brain Res* 233: 317-336, 1982.

Richter DW. Generation and maintenance of the respiratory rhythm. *J Exp Biol* 100: 93-107, 1982.

Ritter B and Zhang W. Early postnatal maturation of GABAA-mediated inhibition in the brainstem respiratory rhythm-generating network of the mouse. *Eur J Neurosci* 12: 2975-2984, 2000.

Rivera C, Voipio J, Payne JA, Ruusuvuori E, Lahtinen H, Lamsa K, Pirvola U, Saarma M and Kaila K. The K+/Cl- co-transporter KCC2 renders GABA hyperpolarizing during neuronal maturation. *Nature* 397: 251-255, 1999.

Ruangkittisakul A, Schwarzacher SW, Secchia L, Poon BY, Ma Y, Funk GD and Ballanyi K. High sensitivity to neuromodulator-activated signaling pathways at physiological [K+] of confocally imaged respiratory center neurons in on-line-calibrated newborn rat brainstem slices. *J Neurosci* 26: 11870-11880, 2006.

Saywell SA and Feldman JL. Dynamic interactions of excitatory and inhibitory inputs in hypoglossal motoneurones: respiratory phasing and modulation by PKA. *J Physiol* 554: 879-889, 2004.

Schoppa NE. Synchronization of olfactory bulb mitral cells by precisely timed inhibitory inputs. *Neuron* 49: 271-283, 2006.

Seager MA, Johnson LD, Chabot ES, Asaka Y and Berry SD. Oscillatory brain states and learning: Impact of hippocampal theta-contingent training. *Proc Natl Acad Sci U S A* 99: 1616-1620, 2002.

Sears TA and Stagg D. Short-term synchronization of intercostal motoneurone activity. *J Physiol* 263: 357-381, 1976.

Sebe JY, Eggers ED and Berger AJ. Differential effects of ethanol on GABA(A) and glycine receptor-mediated synaptic currents in brain stem motoneurons. *J Neurophysiol* 90: 870-875, 2003.

Sebe JY, van Brederode JF and Berger AJ. Inhibitory synaptic transmission governs inspiratory motoneuron synchronization. *J Neurophysiol* 96: 391-403, 2006.

Shao XM and Feldman JL. Respiratory rhythm generation and synaptic inhibition of expiratory neurons in pre-Botzinger complex: differential roles of glycinergic and GABAergic neural transmission. *J Neurophysiol* 77: 1853-1860, 1997.

Singer JH, Talley EM, Bayliss DA and Berger AJ. Development of glycinergic synaptic transmission to rat brain stem motoneurons. *J Neurophysiol* 80: 2608-2620, 1998.

Smith JC, Ellenberger HH, Ballanyi K, Richter DW and Feldman JL. Pre-Botzinger complex: a brainstem region that may generate respiratory rhythm in mammals. *Science* 254: 726-729, 1991.

Smith JC and Feldman JL. In vitro brainstem-spinal cord preparations for study of motor systems for mammalian respiration and locomotion. *J Neurosci Methods* 21: 321-333, 1987.

Solomon IC. Connexin36 distribution in putative CO2-chemosensitive brainstem regions in rat. *Respir Physiol Neurobiol* 139: 1-20, 2003.

Solomon IC, Chon KH and Rodriguez MN. Blockade of brain stem gap junctions increases phrenic burst frequency and reduces phrenic burst synchronization in adult rat. *J Neurophysiol* 89: 135-149, 2003.

Steriade M. Coherent oscillations and short-term plasticity in corticothalamic networks. *Trends Neurosci* 22: 337-345, 1999.

Steriade M, McCormick DA and Sejnowski TJ. Thalamocortical oscillations in the sleeping and aroused brain. *Science* 262: 679-685, 1993.

Stopfer M, Bhagavan S, Smith BH and Laurent G. Impaired odour discrimination on desynchronization of odour-encoding neural assemblies. *Nature* 390: 70-74, 1997.

Suthers GK, Henderson-Smart DJ and Read DJ. Postnatal changes in the rate of high frequency bursts of inspiratory activity in cats and dogs. *Brain Res* 132: 537-540, 1977.

Suzue T. Respiratory rhythm generation in the in vitro brain stem-spinal cord preparation of the neonatal rat. *J Physiol* 354: 173-183, 1984.

Talley EM, Lei Q, Sirois JE and Bayliss DA. TASK-1, a two-pore domain K+ channel, is modulated by multiple neurotransmitters in motoneurons. *Neuron* 25: 399-410, 2000.

Thoby-Brisson M and Ramirez JM. Identification of two types of inspiratory pacemaker neurons in the isolated respiratory neural network of mice. *J Neurophysiol* 86: 104-112, 2001.

Travers JB, Yoo JE, Chandran R, Herman K and Travers SP. Neurotransmitter phenotypes of intermediate zone reticular formation projections to the motor trigeminal and hypoglossal nuclei in the rat. *J Comp Neurol* 488: 28-47, 2005.

Tryba AK, Pena F and Ramirez JM. Stabilization of bursting in respiratory pacemaker neurons. *J Neurosci* 23: 3538-3546, 2003.

Viana F, Gibbs L and Berger AJ. Double- and triple-labeling of functionally characterized central neurons projecting to peripheral targets studied in vitro. *Neuroscience* 38: 829-841, 1990.

Vicini S, Ferguson C, Prybylowski K, Kralic J, Morrow AL and Homanics GE. GABA(A) receptor alpha1 subunit deletion prevents developmental changes of inhibitory synaptic currents in cerebellar neurons. *J Neurosci* 21: 3009-3016, 2001.

von Euler C. Brain stem mechanisms for generation and control of breathing pattern. In: Handbook of Physiology. Section 3. The Respiratory System. Volume 2. Control of Breathing. Part 1., edited by Fishman AP, Cherniack NS, Widdicombe JG and Geiger SR. Bethesda, Maryland: American Physiological Society, 1986, p. 1-67.

Yasuda K, Robinson DM, Selvaratnam SR, Walsh CW, McMorland AJ and Funk GD. Modulation of hypoglossal motoneuron excitability by NK1 receptor activation in neonatal mice in vitro. *J Physiol* 534: 447-464, 2001.

Vita

Joy Yoshiko Sebe

Education

2000-2006 Ph.D. in Neurobiology and Behavior
University of Washington, Seattle, Washington

2005 B.A. in Biology with Honors, *cum laude*
Occidental College, Los Angeles, CA

Publications

J. Y. Sebe and A.J. Berger. Possible Premotor Origin for the Generation of Synchronous Oscillation within the Slice. In preparation.

A.J. Berger and J.Y. Sebe. Developmental Effects of Ketamine on Inspiratory Hypoglossal Nerve Activity Studied *In Vivo* and *In Vitro*. Provisionally accepted. *Respir Physiol and Neurobiol.*

J.Y. Sebe, J.F. vanBrederode and A.J. Berger. Inhibitory Synaptic Transmission Governs Inspiratory Motoneuron Synchronization. *J. Neurophysiol* 96: 391-403, 2006.

J.A. O'Brien, J.Y. Sebe, and A.J. Berger. Modulation of $GABA_A$ and Glycine Receptor Mediated Synaptic Currents by $GABA_B$ Receptors in Brainstem Motoneurons. *Respir Physiol Neurobiol* 141: 35-45, 2004.

J.Y. Sebe, E.D. Eggers, and A.J. Berger. Differential Effects of Ethanol on $GABA_A$ and Glycine Receptor Mediated Synaptic Currents in Brainstem Motoneurons. *J Neurophysiol* 90: 870-875, 2003.

Abstracts

A.J. Berger and J.Y. Sebe. Developmental Effects of Ketamine on Inspiratory Hypoglossal Nerve Activity Studied *In Vivo* and *In Vitro*. Experimental Biology, 2007.

B.D. White, H. Watari, J.T. Ting, J.Y. Sebe, A.M. Wissman, E. Cherny, R.A. McDevitt, T.J. Lambert, J. Meitzen, E.H. Chudler;. Interactive Brain Awareness Week exhibits offer experience learning: a model for teaching concepts in neuroscience. Society for Neuroscience, 2006.

J.Y. Sebe, J.F. vanBrederode and A.J. Berger. GABAergic and Glycinergic Transmission Modulate Inspiratory Motoneuron Synchronization. Society for Neuroscience, 2005.

J.Y. Sebe and A.J. Berger. $GABA_A$ and Glycine Receptor-Mediated Synaptic Transmission Differentially Modulate Inspiratory Motoneuron Synchronization. Society for Neuroscience, 2004.

J.Y. Sebe, J.A. O'Brien, and A.J. Berger. Modulation of $GABA_A$ and Glycine Receptor-Mediated Synaptic Currents by $GABA_B$ Receptors in Brainstem Motoneurons. Society for Neuroscience, 2003.

J. Y. Sebe, E.D. Eggers, and A.J. Berger. Differential Effects of Ethanol on $GABA_A$ versus Glycine Receptor Mediated Synaptic Currents in Brainstem Motoneurons. Society for Neuroscience, 2002.